

Influence of Anthropogenic Nutrient Inputs on Rates of Coastal Ocean Nitrogen and Carbon Cycling in the Southern California Bight, USA

Karen McLaughlin¹, Meredith Howard¹, George Robertson², Carly Beck¹, Minna Ho¹, Faycal Kessouri¹, Nikolay Nezlin¹, Martha Sutula¹, and Stephen Weisberg¹

¹Southern California Coastal Water Research Project

²Orange County Sanitation District

November 24, 2022

Abstract

Coastal nitrogen (N) enrichment is a global environmental problem that can influence acidification, deoxygenation, and subsequent habitat loss in ways that can be synergistic with global climate change impacts. In the Southern California Bight, an eastern boundary upwelling system, modeling of wastewater discharged through ocean outfalls has shown that it effectively doubles N loading to urban coastal waters. However, effects of wastewater outfalls on biogeochemical rates of primary production and respiration, key processes through which coastal acidification and deoxygenation are manifested, have not been directly linked to observed trends in ambient chlorophyll *a*, oxygen and pH. In this paper, we compare observations of nutrient concentrations and forms, as well as rates of nitrification, primary production, and respiration, in areas within treated wastewater effluent plumes compared to areas spatially distant from ocean outfalls where we expected minimum influence of the plume. We document that wastewater nutrient inputs have an immediate, local effect on nutrient stoichiometry, elevating ammonium and nitrite concentrations and increasing dissolved nitrogen: phosphorus ratios, as well as increasing rates of nitrification within the plume. We did not observe a near plume effect on nitrate assimilation into the biomass, primary production, chlorophyll *a*, respiration, or dissolved oxygen concentration, suggesting any potential impact from wastewater on these processes is moderated by offshore factors, notably mixing of water masses. These results indicate that a “reference-area” approach, wherein stations within or near the zone of initial dilution (ZID) from the wastewater outfall are compared to stations farther afield (reference areas) to assess contaminant impacts, is insufficient to document regional scale impacts of nutrients. Understanding of the complex interactions between local, regional, and global drivers on coastal eutrophication requires coupled observational-numerical modeling approaches where numerical models are carefully validated with observed state and rate data to develop effective, evidence-based solutions to coastal eutrophication.

**Influence of Anthropogenic Nutrient Inputs on Rates of Coastal Ocean Nitrogen and Carbon
Cycling in the Southern California Bight, USA**

Karen McLaughlin^{1*}, Meredith D.A. Howard^{1,2}, George Robertson³, Carly D.A. Beck^{1,4}, Minna
Ho¹, Fayçal Kessouri¹, Nikolay P. Nezlin^{1,5}, Martha Sutula¹, Stephen B. Weisberg¹

*Corresponding author

¹Southern California Coastal Water Research Project

²now at: California Region 5, Central Valley Regional Water Quality Control Board

³Orange County Sanitation District

⁴now at: California Department of Fish and Wildlife

⁵now at: RBR, Ltd.

For submission to Elementa
<https://www.elementascience.org/>

Abstract

Coastal nitrogen (N) enrichment is a global environmental problem that can influence acidification, deoxygenation, and subsequent habitat loss in ways that can be synergistic with global climate change impacts. In the Southern California Bight, an eastern boundary upwelling system, modeling of wastewater discharged through ocean outfalls has shown that it effectively doubles N loading to urban coastal waters. However, effects of wastewater outfalls on biogeochemical rates of primary production and respiration, key processes through which coastal acidification and deoxygenation are manifested, have not been directly linked to observed trends in ambient chlorophyll *a*, oxygen and pH. In this paper, we compare observations of nutrient concentrations and forms, as well as rates of nitrification, primary production, and respiration, in areas within treated wastewater effluent plumes compared to areas spatially distant from ocean outfalls where we expected minimum influence of the plume. We document that wastewater nutrient inputs have an immediate, local effect on nutrient stoichiometry, elevating ammonium and nitrite concentrations and increasing dissolved nitrogen: phosphorus ratios, as well as increasing rates of nitrification within the plume. We did not observe a near plume effect on nitrate assimilation into the biomass, primary production, chlorophyll *a*, respiration, or dissolved oxygen concentration, suggesting any potential impact from wastewater on these processes is moderated by offshore factors, notably mixing of water masses. These results indicate that a “reference-area” approach, wherein stations within or near the zone of initial dilution (ZID) from the wastewater outfall are compared to stations farther afield (reference areas) to assess contaminant impacts, is insufficient to document regional scale impacts of nutrients. Understanding of the complex interactions between local, regional, and global drivers on coastal eutrophication requires coupled observational-numerical modeling approaches where numerical models are carefully validated with observed state and rate data to develop effective, evidence-based solutions to coastal eutrophication.

1 Introduction

2
3 Globally, offshore ocean outfalls have been considered an effective and reliable strategy
4 for disposing of treated industrial and domestic wastewater (Wood et al. 1993, Roberts et al.
5 2010). However, wastewater effluent released through these outfalls are rarely treated to
6 remove nutrients and, consequently, they have been implicated in eutrophication of coastal
7 waters (Roberts et al. 2010, Powley et al. 2016, Valiela et al. 2016). Eutrophication can have
8 impacts on coastal habitats that can be synergistic with global changes, such as increasing
9 frequency and occurrence of algal blooms (Howarth et al. 2002, Glibert et al. 2006), coastal
10 acidification (Borges and Gypens 2010, Wallace et al. 2014), and deoxygenation (Rabalais et al.
11 2014, Breitburg et al. 2018) through enhanced heterotrophic respiration rates. Given
12 appropriate light and temperature conditions, eutrophication initially causes a temporary
13 drawdown of CO₂ concentrations at the surface due to the intense biological productivity of the
14 associated algal bloom (Borges and Gypens 2010). Subsequently, eutrophication lowers pH,
15 because it provides conditions for greater heterotrophic respiration rates (i.e., decomposition,
16 also referred to as remineralization) by organisms such as bacteria. This respiration process
17 oxidizes organic matter, draws down local oxygen levels, releases CO₂, and—in extreme cases—
18 can lead to hypoxic dead zones (Diaz and Rosenberg, 2008). The depth of the pH change
19 associated with anthropogenic eutrophication is a function of where organic matter is respired.
20 In many shallow coastal shelf systems, this acidification occurs at or near the bottom
21 sediments, where organic matter is oxidized (Waldbusser et al. 2010, Sunda and Cai 2012). In
22 the absence of global strategies to mitigate coastal ocean changes, local managers are being
23 urged to consider the management of local, land-based nutrient sources to slow the
24 progression of acidification and deoxygenation and their impact on coastal habitats (Kelly et al.
25 2011, Strong et al. 2014, Chan et al. 2016).

26 The role of coastal nutrient discharges and coastal eutrophication in exacerbating
27 coastal acidification and deoxygenation (CAD) is well documented, including the East China Sea
28 and the Gulf of Mexico (Cai et al. 2011), the Baltic Sea (Sunda and Cai 2012), the nearshore
29 regions of the North Sea (Provoost et al. 2010), and the Chesapeake Bay (Waldbusser 2011).

1 However, in an Eastern Boundary Upwelling System (EBUS), strong upwelling and vigorous
2 surface currents have been thought to limit the impacts of local anthropogenic nutrient inputs
3 (Chavez and Messié 2009, Capone and Hutchins 2013, Fennel and Testa 2019). Recent evidence
4 from the Southern California Bight (SCB) has challenged this thinking along this highly urbanized
5 coastline. In the SCB, on an annual basis, 92% of terrestrial N flux is wastewater effluent from
6 Publicly Owned Treatment Works (POTWs), most of which is discharged directly into coastal
7 waters via a relatively small number of outfall pipes (Sutula et al. 2020). Modeled outfall N
8 loads are roughly equivalent to those from upwelling in urbanized sections of the coast,
9 effectively doubling N loading to the shelf (Howard et al. 2014). These inputs have an
10 immediate, local effect on nitrification rates as high concentrations of wastewater ammonium
11 are rapidly nitrified in the subsurface plumes (McLaughlin et al. 2017). More broadly,
12 observational evidence has shown an increase in the extent of algal blooms in the SCB over the
13 last decade, with chronic blooms documented in areas co-located with major inputs of
14 anthropogenic nutrients (Schnetzler et al. 2007a, Nezlin et al. 2012, Schnetzler et al. 2013).
15 Analysis of a decade of quarterly ocean surveys across the central and northern SCB have
16 shown a significant decrease in dissolved oxygen (DO) concentrations (Bograd et al. 2008), and
17 the rate of decline in the nearshore, proximal to treated wastewater effluent outfalls, has been
18 faster than offshore regions (Booth et al. 2014). However, these regional-scale observations
19 can also be influenced by climate change and Pacific Basin-scale drivers (Booth et al. 2014,
20 Nezlin et al. 2018) and ambient chlorophyll *a*, DO and pH have not been specifically linked to an
21 effect of wastewater outfalls on biogeochemical rates of primary production and respiration –
22 key processes through which CAD are manifested.

23 In this paper, we quantified nutrient concentrations, forms, and key rates of carbon and
24 nitrogen cycling that ultimately influence processes leading to eutrophication and CAD both
25 within wastewater plumes and in areas spatially distant from plumes. We also explored the
26 environmental factors that may be influencing rates, including seasonal and interannual
27 variability linked to the influence of upwelling. Finally, we employed stable isotope tracers to
28 further track relationships and patterns in N and C biogeochemical cycling in these coastal
29 zones. We focused on the effect of wastewater N because the SCB is largely N-limited (Thomas

et al. 1974, Cullen and Eppley 1981) and wastewater point source discharges dominate anthropogenic sources (Howard et al. 2014) and contain high concentrations of nitrogenous species. As a core part of our study design, observations of ambient ocean state and rates were made in two types of regions defined by the probability of plume impact: 1) “nearfield” regions, defined as the region of active effluent plume mixing and dispersion within 10 km of the outfall and 2) “farfield” regions, defined as the region where ambient ocean flow and biogeochemical conditions dominate and the effluent plume is expected to exert minimum influence on carbon and nitrogen cycling.

The value of such observations extends beyond testing of the hypothesis of an effect of wastewater plumes on watercolumn biogeochemical parameters (pH, dissolved oxygen, chlorophyll *a*) and rates of nutrient and carbon cycling. To support California's climate action strategies, a spatially-explicit, 3-dimensional numerical ocean model of the SCB was developed and is being applied to examine the relative effects of climate change, natural climate cycles, and local terrestrial and atmospheric carbon and nutrient inputs (Deutsch et al. in review). However, in order to support conversations on the utility of nutrient management as a climate change mitigation strategy, such models must be carefully validated against observations of biogeochemical state and rate data. Inadequate numerical model validation has been identified as a significant barrier to effective, evidence-based solutions to coastal eutrophication (Boesch 2019). Models must not only successfully reproduce observed state data, they must also successfully reproduce observed biogeochemical rate data, ensuring that the model is predicting the appropriate state variables for the right reasons. Thus, these observations are part of a coupled observational-numerical modeling approach characterizing the effect of local nutrient and carbon inputs on SCB coastal habitats, laying the foundation for evidence-based solutions for CAD.

Materials and Methods

Study Region

The Southern California Bight (SCB) is the bend in the coastline between Point Conception (~34° 34'N) and the U.S.-Mexico International Border (~32° 32'N). It is situated in the California Current System (CCS) on the U.S. Pacific Coast. As an EBUS, the SCB is a biologically productive region of high economic and ecological importance. Seasonal spring upwelling of nutrient-rich deep water maintains high rates of biological productivity over broad scales. At the same time, upwelling draws water masses that are low in DO, pH, and carbonate saturation state (Ω_{Ar}) onto the shelf and into the photic zone (Sutton et al. 2017). Southern California has a Mediterranean climate with surface runoff confined mostly to the winter, rainy season. The SCB is home to one of the most densely populated coastal regions in North America, where the discharges of treated (advanced primary or secondary) wastewater from a population of 20 million people are released to the coastal zone via ocean outfalls, along with the urban and agricultural runoff from 72 rivers (Sutula et al. 2020). Modeling efforts have shown that these nutrient sources rival natural upwelling in magnitude (Howard et al., 2014), roughly doubling available N to nearshore coastal waters on an annual basis.

Study Design

The study was designed to characterize effects of wastewater plumes on state and rate variables in regions nearfield (within-plume) and farfield (spatially distant) from ocean outfalls where treated wastewater effluent is discharged to the highly urbanized, central portion of the Bight (Figure 1). We hypothesized that chemical and biological rates and water chemistry would differ between areas near ocean outfalls (nearfield), where treated wastewater plume was detected, compared to farfield, “reference” areas, where the plume could not be detected. Selection of nearfield and farfield locations was informed by previous studies that used colored dissolved organic matter (CDOM) as a tracer of effluent plume (Rogowski et al. 2013, Nezlin et al. 2020); as a rule of thumb, nearfield stations were generally within 10 km of the outfalls, while farfield stations were greater than 10 km away.

We compared water column nutrient profiles and stable isotopic compositions, as well as rates of nitrification, primary production and respiration in nearfield and farfield regions, as well as relationships between parameters and rates, and seasonal and interannual differences thereof. Four sub-regions were sampled, including two nearfield sub-regions near Orange County Sanitation District's (OCSD) and Los Angeles County Sanitation District's (LACSD) ocean outfalls, a nearshore, farfield sub-region off the coast of northern San Diego County (Camp Pendleton), and an offshore, farfield sub-region off the coast of Los Angeles and Orange Counties (Table 1 and Figure 1). Two stations were sampled in each sub-region for the full suite of measurements and rate analyses. For the nearfield regions, sampling was dynamic and varied based on currents to enable sampling within the plume. A fixed sampling station was located directly over the outfall pipe and a second site, which varied according to currents, was located a short distance from the outfall, but still within the plume. Further, one additional fixed station was sampled in each effluent-plume sub-region for water column nutrients and stable isotope analysis only (no rate data). For the farfield coastal subregion, one station was located on the continental shelf and the other on the shelf-break. For the offshore farfield subregion, one was located at the San Pedro Ocean Time Series (SPOTS) station (offshore of LACSD's outfall) and the other at the California Cooperative Oceanic Fisheries Investigations (CalCOFI) sample station 90.30 (offshore of OCSD's outfall), both within the San Pedro Basin.

Comparisons and relationships were investigated seasonally, both when wastewater discharge was anticipated to constitute a minor fraction of the total N pool (Spring upwelling period) and a major fraction (late Summer, when the water column is stratified). Four seasons were collected over two years: late Summer stratification in 2014 and 2015, and Spring upwelling in 2015 and 2016. Cruises and rate measurements were conducted over a four-week period in each season; one sub-region sampled per week.

Sample Collection

Vertical profiles were collected at each station using a Sea-Bird Electronics, Inc., SBE911plus (24 Hz) or SBE-25 (8 Hz) conductivity-temperature-depth (CTD) system, measuring a

1 suite of oceanographic properties including pressure, temperature, salinity, colored dissolved
2 organic matter (CDOM), dissolved oxygen, pH, and chlorophyll fluorescence and transmissivity.
3 In addition to the experimental stations, CTD casts were also taken at several stations in the
4 nearfield sub-regions to map the location of the plume and regional hydrodynamics at the time
5 of sampling (Figure SI.1). The profiles were averaged to 1 m bins. Regional climatologies of
6 temperature, salinity, dissolved oxygen, chlorophyll *a*, and CDOM were generated by
7 interpolation using the Barnes algorithm (Koch et al. 1983) from the R package “oce” (Kelley
8 and Richards 2017).

9 Discrete samples were collected from Niskin bottles (1.5 and 3 L) on a rosette deployed
10 with the CTD sensor package. Sampling was adaptive at each site, with sample depths
11 determined from downcast CTD observations to identify key oceanographic features at each
12 station (CDOM and chlorophyll *a* maxima). Generally, samples were collected from 5 depths at
13 the stations > 50 m depth: the surface, subsurface chlorophyll maximum layer (depth of highest
14 recorded chlorophyll fluorescence), the center of the thermocline (mixed layer, where the
15 temperature gradient exceeds $-0.3\text{ }^{\circ}\text{C m}^{-1}$), below the thermocline, and at the “bottom” (2-5 m
16 from the sediment surface or the end of the rosette cable, which was either 200 m [OCSD,
17 LACSD] or 300 m [Camp Pendleton]). At shallower stations, four samples were collected from
18 the surface, subsurface chlorophyll maximum, the thermocline, and the bottom. For the
19 nearfield sub-regions, the station over the outfall remained fixed throughout the study, but the
20 “off-outfall/second nearfield” station varied based on currents and was identified using CTD
21 profiles of CDOM from several stations (Figure SI.1). CDOM has been shown to be a reasonable
22 tracer for subsurface effluent plumes (Rogowski et al. 2012, Rogowski et al. 2013, Nezlin et al.
23 2020).

24 Field water samples were transferred from the Niskin bottles using acid-washed Tygon
25 tubing into acid-washed 2 L high density polyethylene (HDPE) bottles that were triple rinsed
26 with sample water before filling. Both LACSD and OCSD also supplied samples of effluent for
27 analysis prior to each sampling event in their respective nearfield subregions. These samples
28 were collected as a composite over 24 hours in an acid washed 1 L HDPE bottle. Effluent was
29 stored at 4 °C while the composite was generated.

Sub-samples from both field water and effluent were collected for the suite of dissolved inorganic nutrients (nitrate+nitrite, nitrite, ammonium, and ortho-phosphate), total dissolved nitrogen and phosphorus (TDN, TDP), and dual nitrogen and oxygen isotope ratios for dissolved nitrate. In addition, field water was sub-sampled for particulate organic matter concentrations (particulate nitrogen, particulate phosphorus, and particulate organic carbon), stable isotope ratios of carbon and nitrogen of particulate organic matter, and chlorophyll *a*. Subsamples were frozen immediately. Suspended particulate samples were collected by vacuum filtration onto pre-combusted (450 °C for 4 hours) glass fiber filters (Whatman GF/F). Suspended particulate samples were sub-sampled from the whole water sample and stable isotope analyses and were filtered onboard the cruise and frozen immediately. Filters were collected into snap-close petri dishes and stored in Ziploc bags on ice in the dark for transport. Filters in the petri dishes were dried at 50 °C in the dark until analysis.

Sub-samples for nutrient and nitrate stable isotope analysis were hand-filtered through a 0.45 µm polycarbonate filter (Millipore) and collected in triple-rinsed, 60 mL HDPE amber bottles, stored on ice for transport to the laboratory, and frozen until analysis (Wankel et al. 2006, Wankel et al. 2007, Santoro et al. 2010). Whole water for primary production and nitrification rate incubations were collected directly into acid-washed, triple-rinsed, 2 L HDPE bottles and stored on ice in the dark until the incubations could begin in the laboratory within 6 hours of collection. Whole water for respiration rates was collected into 300 mL borosilicate glass biological oxygen demand bottles that were overfilled with twice the volume of the bottle. Whole water for nitrogen uptake kinetics experiments was collected into 20 L acid-cleaned polycarbonate (Nalgene) carboys. Water samples for the rate experiments (primary production, respiration, and nitrification) were stored on ice and in the dark until they were brought back to the lab for experimental preparation.

Laboratory Analyses

Nutrient concentrations. Discrete samples were analyzed for a suite of dissolved nutrients. Nitrate + nitrite, soluble reactive phosphate, and ammonium were analyzed using flow injection analyses (FIA, Lachat Instruments, QuikChem 8000 at the Marine Science

Institute, at the University of California, Santa Barbara), ammonium was also measured following the protocols of Holmes et al. (1999), total N (TN) and phosphorus (TP) samples were analyzed following persulfate digestion (Patton and Kryskalla 2003) using FIA. A relative assessment of nutrient limitation, N^* , was calculated, which represents the deviation in “Redfield” N:P stoichiometry due to additional sources and sinks of nitrate (Deutsch et al. 2001):

$$N^* = [NO_3^-] - (16 * [PO_4^{3-}]) + 2.9 \quad (\text{Eq 1}).$$

Positive N^* values reflect regions with a source of nitrate (via nitrogen fixation) and negative N^* reflects a sink of nitrate (due to denitrification). Values near zero are consistent with “Redfieldian” assimilation and nitrification of organic matter or that source and loss terms are balanced (Gruber and Sarmiento 1997).

Stable Isotope Analyses. The stable isotopic compositions of dissolved nitrate ($\delta^{15}N_{NO_2+NO_3}$ and $\delta^{18}O_{NO_3}$), ammonium ($\delta^{15}N_{NH_4}$), and suspended particulate matter ($\delta^{15}N_{PN}$ and $\delta^{13}C_{PN}$) are natural tracers of N sources and cycling in the ocean. Variation in the isotopic composition is attributable to distinct source signatures and the mass dependent isotopic discriminations associated with various biogeochemical transformations that constitute the marine N cycle. Because each pathway causes a characteristic shift in isotope composition of the products and reactants, the isotopic composition of the dissolved and particulate pools can provide useful information on the mechanism of these transformations (Sigman et al. 2005, Wankel et al. 2007, Sugimoto et al. 2009).

The preparation and isotope analysis ($\delta^{15}N$, $\delta^{18}O$) of dissolved nitrate in discrete water samples was performed using a bacterial denitrification assay (Sigman et al. 2001, Casciotti et al. 2002). Samples with at least 0.002 mg/kg as N were analyzed by bacterial conversion of nitrate to nitrous oxide and sub-sequent measurement on a continuous flow isotope ratio mass spectrometer (Sigman et al., 2001; Casciotti et al., 2002; Coplen et al., 2007). Isotope ratios of $^{15}N/^{14}N$ and $^{18}O/^{16}O$ were measured using a ThermoFinnigan GasBench + PreCon trace gas concentration system interfaced to a ThermoScientific Delta V Plus isotope-ratio mass spectrometer at the Stable Isotope Laboratory at the University of California, Riverside.

Dissolved ammonium was extracted from 250 mL of wastewater effluent onto glass fiber filter “traps” (Holmes et al. 1998, Hannon and Böhlke 2008) and the isotope ratios of $^{15}\text{N}/^{14}\text{N}$ were measured using a coupled Costech Elemental Analyzer with a Finnigan Delta Plus Advantage in Continuous Flow Mode at the Stable Isotope Laboratory at the University of California, Riverside. The isotope ratios of $^{15}\text{N}/^{14}\text{N}$ and $^{13}\text{C}/^{12}\text{C}$ from suspended particulate matter and from net tows collected on precombusted Whatman GF/F were measured using a coupled Costech Elemental Analyzer with a Finnigan Delta Plus Advantage in Continuous Flow Mode at the Stable Isotope Laboratory at the University of California, Riverside. Isotope ratios are reported relative to standards: N_2 in air for $\delta^{15}\text{N}$, Vienna Standard Mean Ocean Water (VSMOW) for $\delta^{18}\text{O}$, and Vienna Pee Dee Belemnite (VPDB) for $\delta^{13}\text{C}$. The standard deviation of replicate standards for particulate material $\delta^{13}\text{C}$ was 0.084 ‰ and $\delta^{15}\text{N}$ was 0.165 ‰, and the relative percent difference between measured standards and reference values was 0.32% and 0.88%, respectively. The standard deviation of replicate standards for dissolved nitrate $\delta^{18}\text{O}$ was 0.17 ‰ and $\delta^{15}\text{N}$ was 0.15 ‰, and the relative percent difference between measured standards and reference values was 0.46% and 0.04%, respectively.

Rate Measurements

Primary production rate measurements. Short-term incubations of natural plankton communities were conducted to determine rates of primary production using radioactive ^{14}C labeled compounds, expressed as $\text{mg C m}^{-3} \text{ day}^{-1}$ or integrated vertically to units of $\text{mg C m}^{-2} \text{ day}^{-1}$. Primary production was estimated at four depths bracketing the euphotic zone (including light levels from 95% to 1%) from ^{14}C uptake using a simulated *in situ* technique in which the assimilation of dissolved inorganic carbon by phytoplankton yields a measure of the rate of photosynthetic primary production in the euphotic zone (Anderson et al. 2006, Brzezinski and Washburn, 2011). Water was collected from Niskin bottles into 2 L HDPE bottles wrapped in black electrical tape and kept in darkened coolers until transported to the laboratory. Depths included: surface, the chlorophyll maximum, the center of the thermocline, and the 1% light level (three times the Secchi depth). Subsamples from each depth were separated into two acid-cleaned 250 mL polycarbonate bottles; one bottle was wrapped in black electrical tape to

measure dark ^{14}C uptake and the other was left open to light but darkened to expected ambient light levels using a neutral density screen. Bottles were incubated for 24 hours after inoculation with ^{14}C sodium bicarbonate in incubators placed outside in ambient light in the Southern California Coastal Water Research Project facility, held at recorded *in situ* seawater temperatures by circulating incubator water through chillers. At the end of incubations total radioactivity in each sample was determined by adding 250 μL of incubated seawater to 250 μL of β -phenethylamine in a 20 mL glass scintillation vial followed by 10 mL of Ultima Gold XR scintillation cocktail. Each vial was shaken vigorously for 30 s and ^{14}C activity assayed after bubbles had cleared and chemoluminescence had subsided (~2 hours) by a liquid scintillation counter using an internal quench curve. A 50 mL subsample of incubated water was also filtered through a pre-combusted 25 mm Whatman GF/F filter. Filters were placed in individual 20 mL glass scintillation vials and 0.25 mL of 0.5 N HCl was pipetted onto each filter in a fume hood to drive off excess tracer. Vials were left uncapped for a minimum of 7 hours, and 10 mL of Ultima Gold XR scintillation cocktail was added to each vial, the vials capped and shaken, and ^{14}C activity was analyzed by scintillation counting on a scintillation counter using an internal quench curve. Primary productivity rates in both the light and dark incubations were calculated as described by Anderson et al. (2006) and Brzezinski and Washburn (2011). Daily primary production ($\text{g C m}^{-3} \text{ d}^{-1}$) was calculated as the difference in productivity between light and dark bottles. Productivity-to-biomass ratio was calculated as the daily primary productivity ($\text{g C m}^{-3} \text{ d}^{-1}$) per unit chlorophyll *a* (g chl a m^{-3}) with units of $\text{gC (g chl a)}^{-1} \text{ d}^{-1}$. Integrated rates of productivity were calculated using the trapezoidal method.

Respiration rate measurements. Respiration rates were measured at four depths: the chlorophyll maximum, the middle of the thermocline, below the thermocline, and 2 m above the bottom/end of the CTD cable. Whole water was collected from Niskin bottles into 300 mL glass bottles, each of which was wrapped in black electrical tape, using acid-cleaned Tygon tubing, overfilling each bottle with at least twice the volume. Three bottles were collected for respiration rate measurements at each depth. An additional 50 mL syringe of whole water was collected from each Niskin bottle and held in a cooler. An initial dissolved oxygen concentration

(mg O L⁻¹) and percent oxygen saturation was recorded in the field for each bottle using a YSI ProDO optical dissolved oxygen probe, immediately after bottles were filled. Because the probe displaced some water from each bottle, water was replaced with whole water from the syringe to eliminate headspace in each bottle. Bottles were then stoppered and placed in refrigerated units held at *in situ* water temperatures. Bottles were incubated for 24-48 hours and a final dissolved oxygen concentration (mg L⁻¹) and percent oxygen saturation in each bottle was recorded. Respiration rates were calculated for each depth at *in situ* temperatures as the difference between time zero oxygen concentrations and final incubated oxygen concentrations.

Nitrification rate measurements: Nitrification is the sequential oxidation of NH₄⁺ to NO₃⁻ via NO₂⁻. Nitrification rates were determined by measuring the accumulation of ¹⁵N in the dissolved nitrate pool following addition of isotopically-enriched ammonium to bottle incubations (Santoro et al. 2010). Water was collected from Niskin bottles into 2 L HDPE bottles at four depths: the chlorophyll maximum layer, the middle of the thermocline, below the thermocline, and 2 m above the bottom/end of the CTD cable. Subsamples from this initial sample were separated into three 500 mL acid-washed polycarbonate bottles wrapped in black tape. An enriched (99%) tracer of ¹⁵N-ammonium chloride was added to a final concentration of 100 nM to two of the bottles and a third bottle without the tracer served as a control. Not knowing ammonium concentrations beforehand, we targeted this concentration to minimize impact on nitrogen cycling within the bottles. The range of percentage labeled ammonium from 0.01 to 1.5%, with a median value of 0.1%. Bottles were incubated in the dark to minimize N uptake by phytoplankton and as close to *in situ* temperature conditions as possible (within ± 2°C) in a series of refrigerated incubator units. For reference, Q₁₀ values for nitrification are on the order of 2-3 (Henriksen 1988). Subsamples of 50 mL each were collected at four-time points (approximately 0, 12, 24, and 36 hours post spike addition), syringe filtered through 0.45 µm filters and frozen until analysis for dissolved nitrate concentration and the isotopic composition of nitrate (δ¹⁵N_{NO2+NO3}) as described above. Potential nitrification rates were determined by modeling the ¹⁵N and ¹⁴N contents of the combined nitrate and nitrite pool with

inputs from the labeled ammonium pool and outputs through nitrate and nitrite uptake as described in Santoro et al. (2010). Data fitting for the ^{15}N and ^{14}N values measured at each time point was performed by non-linear least squares regression method using MATLAB 8.2 and Statistics Toolbox 8.3 (The MathWorks, Inc.).

Statistical Analysis

In order to understand relationships between state variables and rates we employed several statistical techniques: Kruskal Wallis, Spearman Rank, and Random Forest regression. To characterize relationships between variables, which were often non-linear, we employed Kruskal Wallis and Spearman Rank nonparametric measures of rank correlation using the R package “Hmisc” (Harrell, 2014). We used Random Forest modeling to characterize variable importance in constraining the variance of rate measurements. Random forest modeling, a machine-learning statistical method which combines many classification trees to produce a more accurate classification (Breiman 2001, Cutler et al. 2007) and has been found to be a robust tool for interpreting ecological datasets (Prasad et al. 2006, Cutler et al. 2007). Random forests provide several metrics that aid in interpretation of multivariable datasets. Variable importance can be evaluated based on how much worse the prediction would be if the data for that predictor were permuted randomly. The resulting tables can be used to compare relative importance among predictor variables (Prasad et al. 2006). Random Forests were conducted using the R package “randomForest” (Law and Weiner 2012).

Results

Wastewater Effluent Characterization

Throughout the study, the effluent nutrient concentrations, isotope ratios, and discharge rates at each outfall were slightly variable (Table 2). Over the study period, both agencies’ effluent discharge rate decreased slightly, a part of a long-term trend related to increasing water use efficiency and reduced water consumption in California. During this same time, LACSD discharged an average of 4.1×10^7 ($\pm 4.5 \times 10^6$) grams of inorganic nitrogen per day

1 and OCSD an average of $1.5 \times 10^7 (\pm 3.2 \times 10^6)$ grams of inorganic nitrogen per day. The
2 characteristics of effluent from OCSD and LACSD were different. Ammonium accounted for
3 >99% of LACSD's dissolved inorganic nitrogen (DIN) load and between 55 and 67% of OCSD's
4 DIN load. OCSD's effluent contains more phosphate compared to LACSD, with an average N:P
5 molar ratio of 100:1 for OCSD and 678:1 for LACSD (Table 2). Dissolved inorganic carbon and
6 dissolved organic carbon were highly variable in both agencies' effluent throughout the study
7 period. The stable N isotopic composition of ammonium ($\delta^{15}\text{N}_{\text{NH}_4}$) and nitrate ($\delta^{15}\text{N}_{\text{NO}_2+\text{NO}_3}$)
8 were different for both plants. OCSD had relatively consistent $\delta^{15}\text{N}_{\text{NH}_4}$, with values ranging
9 between 8.6 and 9.1 ‰ and $\delta^{15}\text{N}_{\text{NO}_2}$, with values ranging between 7.5 and 9.1 ‰. LACSD had
10 $\delta^{15}\text{N}_{\text{NH}_4}$ values ranging from 5.1 to 12.4 ‰. The ammonium isotopic composition in LACSD's
11 effluent was linearly related to the concentration of ammonium in the wastewater (R^2 for
12 LACSD is 0.907, $p = 0.049$, and R^2 for OCSD is 0.364, $p = 0.505$). LACSD also had variable
13 $\delta^{15}\text{N}_{\text{NO}_2+\text{NO}_3}$, with values ranging between -9.6 and -2.3 ‰.

15 ***Seasonal Hydrography, Chlorophyll, and DO***

16 There were clear seasonal differences in temperature and salinity throughout the study
17 region (Figures 2, SI.2). Summer surveys were characterized by high surface water
18 temperatures, shallow thermoclines and haloclines (~10-15 m) and large vertical temperature
19 gradients, indicating strong thermal stratification. Spring surveys were characterized by weaker
20 vertical thermal gradients and deeper thermoclines and haloclines (~20-30 m). The wastewater
21 plume was identifiable by both low salinity and high CDOM in both LACSD's and OCSD's
22 nearfield sub-regions at mid-depth. During Spring 2016 there was a cold, high salinity, low DO
23 water mass intruding into the region from depth throughout the Palos Verdes Shelf region, and
24 notably in the OC Offshore station (CALCOFI station 9030).

25 There were no statistically significant differences between DO in nearfield versus far
26 field areas (Kruskal Wallis). Nearfield stations generally had shallower oxyclines compared to
27 the farfield stations, but that is likely due to close proximity to shore compared to most farfield
28 stations, except for CP1 (Figure 2). DO profiles varied seasonally (Figures 2, SI.2). In the
29 Summer, all regions have similar profiles and a narrower range of values in the upper 60 m.

1 During the Spring surveys, DO had a larger range of values in the upper 60 meters, with surface
2 ocean values similar to Summer, but much lower at depth. Spring also had greater variability in
3 the depth to the oxycline among different stations. The lowest DO was in deeper waters and
4 shoaled closer to the surface during Spring (particularly Spring 2016), indicative of upwelling of
5 cold, deep waters, low in DO.

6 There were no consistent differences in chlorophyll fluorescence in nearfield areas
7 compared to farfield. Daytime, chlorophyll fluorescence had a similar vertical structure to DO,
8 with a clear subsurface maximum layer in all seasons (Figure 2). The depth to and magnitude of
9 the subsurface chlorophyll maximum was variable among stations and among seasons. The
10 lowest chlorophyll was during Summer 2015 and the highest during Spring 2015. The highest
11 values during Spring 2015 are associated with the LACSD and OCSD nearfield areas, appearing
12 as a thin subsurface chlorophyll layer (Figure 2). Spring 2016 had a shallow, narrow chlorophyll
13 layer, with no chlorophyll fluorescence associated with the deep, salty water mass present in
14 Spring 2016. Summer 2014 had middling water column chlorophyll that was deeper offshore
15 and shallower nearshore, whereas Summer 2015 had relatively low chlorophyll overall with the
16 most consistency among stations.

17 Sampling occurred over a four-week period for each season and this may have
18 introduced some variability among stations; however, there was no clear pattern within any
19 sampling season of the nearfield stations having consistently different hydrographic conditions
20 relative to the farfield stations that might create bias in the dataset (Figure SI.2).

22 ***Water Column Nutrient Concentrations***

23 *Dissolved Inorganic Nutrients.*

24 Despite the continuous N-load from both wastewater treatment plants, surface
25 dissolved inorganic nitrogen (DIN) concentrations were generally low in all subregions (Figure
26 3), but not completely depleted. Nutrient profiles showed typical low concentrations in surface
27 waters, due to phytoplankton uptake, with increasing concentrations at depth (Figure 3). There
28 were no statistically significant differences in concentration for phosphate and nitrate among
29 stations (Kruskal Wallis, phosphate/nitrate by station type). Vertical profiles of ammonium and

1 nitrite were significantly different between nearfield and farfield regions (Kruskal Wallis,
2 ammonium/nitrite by station type. $P = 5.5e^{-9}$, $1.8e^{-5}$, respectively). High concentrations of
3 ammonium and nitrite were associated with the plume mixing zone (as detected by CDOM) in
4 the nearfield regions, the depth where the plume reaches neutral buoyancy in the water
5 column.
6

Suspended Particulate Nutrients.

Water column suspended particulate nutrients had similar profiles, with the highest concentrations at the surface and decreasing with depth (Figure SI.3). There were no statistically significant differences by station type for particulate nitrogen or phosphate, but particulate carbon was slightly, significantly higher in nearfield stations (Kruskal Wallis, $p = 0.03$). There were also significant differences by season for all particulate parameters (Kruskal Wallis, $p = 0.0008, 0.02, 2.2e^{-16}$, for PC, PN and PP respectively). Spring 2016 was slightly anomalous from the other three seasons, exhibiting higher concentrations in particulate carbon, nitrogen and phosphorus in surface samples relative to the other seasons, perhaps related to the cold, salty water mass intrusion during that season.

Nutrient Ratios.

Nutrient concentrations for particulate matter and dissolved inorganic nutrients were highly correlated, following the Redfield relationship of C:N:P 106:16:1 (Figure 4, Figure SI. 4). N^* showed strong seasonality, with water column values close to 0 during the Spring upwelling periods, whereas the Summer fluctuated between positive N^* values (Summer 2014), indicative of a source of nitrate, and negative N^* values (Summer 2015), indicative of a sink for nitrate (Figure 5, Figure SI. 5). N^* values near zero suggest that there were no large sources of nitrate (e.g., from nitrogen fixation) or sinks (e.g., due to denitrification).

For particulate matter, particulate C and N were highly correlated, with 90% of C:N ratios between 3.8 and 20.0. C:N ratios less than 6 were found throughout the water column and are atypical of phytoplankton and often associated with bacteria (Goldman et al. 1987). C:P and N:P relationships were close to Redfield, with occasional deviations. These deviations were not related to depth (Figure SI.4) and were more closely tied to station type, with nearshore stations (nearfield stations and farfield, coastal stations at Camp Pendleton) having greater variability than farfield, offshore stations. Relatively high particulate P concentrations were not matched by high concentrations in N and C during Spring 2016.

Water Column Isotope Ratios

Stable Isotopic Composition of Dissolved Nitrate. $\delta^{15}\text{N}_{\text{NO}_2+\text{NO}_3}$ values were generally lower in surface waters, increased to a subsurface maximum, before decreasing again. The $\delta^{18}\text{O}_{\text{NO}_3}$ was highest in surface waters and decreased with depth with no obvious maximum (Figure 6). The shapes of profiles for both $\delta^{15}\text{N}_{\text{NO}_2+\text{NO}_3}$ and $\delta^{18}\text{O}_{\text{NO}_3}$ were closely associated with the vertical distribution of nitrate, DO, and chlorophyll.

At low nitrate concentrations nitrate $\delta^{15}\text{N}_{\text{NO}_2+\text{NO}_3}$ values were variable, but asymptote towards values between 7 and 9 ‰ for all sampling periods as the concentration of nitrate, the fraction of nitrate in the DIN pool, and as nitrification rate all increase (Figure 5, Figure SI.5), similar to what has been seen in urban coastal environments (Sugimoto et al. 2009, McLaughlin et al. 2017). There was no significant relationship between $\delta^{15}\text{N}_{\text{NO}_2+\text{NO}_3}$ and N^* , largely because N^* was typically very close to 0 for most sampling stations and events (Figure 5B, Figure SI.5).

Stable Isotopic Composition of Suspended Particulate Matter. The stable isotopic composition of suspended particulate organic carbon ($\delta^{13}\text{C}_{\text{PM}}$) and particulate organic nitrogen ($\delta^{15}\text{N}_{\text{PM}}$) were lower at the surface, increased to a subsurface maximum, and decreased at depth (Figure 6, Figure SI.6). There were no significant differences by station type for any sampling period, but there were some temporal differences in particulate carbon; $\delta^{13}\text{C}_{\text{PM}}$ in Summer 2014 and Spring 2015 were lower than Summer 2015 and Spring 2016 (Figure 6, Figure SI.6). $\delta^{15}\text{N}_{\text{PM}}$ showed an asymptote to values between 4 and 10 ‰ with increasing particulate N concentration and chlorophyll *a* concentration (Figure 5I, Figure SI.7). By contrast, no significant relationship between $\delta^{15}\text{N}_{\text{PM}}$ and particulate N nor $\delta^{15}\text{N}_{\text{NO}_2+\text{NO}_3}$ was observed (Figure 5G,H, Figure SI.7). $\delta^{13}\text{C}_{\text{PM}}$ was also positively correlated with $\delta^{15}\text{N}_{\text{PM}}$ for most stations and seasons and showed an asymptote between -26 and -20 ‰ with increasing particulate carbon concentration and chlorophyll *a* (Figure 5F, Figure SI.8). $\delta^{13}\text{C}_{\text{PM}}$ was also negatively correlated with water column DIN (Figure SI.8).

Primary Production and Respiration

There was large spatial/temporal variability in both primary production and respiration rates (Figure 7A and 7B, Figure SI.9). Primary production rates ranged from 129 to 2842 mg C m⁻² d⁻¹ and respiration rates ranged from 80.55 to 1521 mg O m⁻³ d⁻¹. There was seasonality in primary production for the two farfield offshore stations, with higher production during the Spring, due to upwelling. However, for the nearshore stations (nearfield stations and the farfield, coastal stations at Camp Pendleton), there were no statistically significant differences between station type (nearfield vs farfield) or season in primary production. Similarly, respiration rates offshore were typically higher than nearshore values, but there were no significant differences between the nearfield stations and farfield, coastal stations (Figure 7B). Primary productivity values are similar to what has been reported for the region (Smith et al. 1982, Eppley 1992) with similar seasonality (Mantyla et al. 2008). There were no significant differences between the LACSD nearfield and the OCSD nearfield (Figure SI.9). There was no significant relationship between primary production and respiration for any season (Figure SI.10).

Nitrification

Nitrification rates were highly variable throughout the study ranging from 0.001 to 325 nmol L⁻¹ day⁻¹, with no clear seasonal patterns. Rates were typically higher in samples collected below the thermocline compared to samples collected in the mixed layer and deep chlorophyll *a* maximum (Figure 7C), similar to profiles measured by others (Ward 1987, 2005, Santoro et al. 2010, Smith et al. 2014) and attributed to light inhibition of nitrification in surface waters. Rates were highest in nearshore stations (nearfield stations and the farfield, coastal stations at Camp Pendleton) compared to the two offshore stations and were typically higher in nearfield areas relative to farfield areas. There were no significant differences between LACSD and OCSD nearfield stations (Figure SI.9).

Discussion

Anthropogenic nutrient discharges into coastal waters can drive significant biogeochemical changes and local managers are being urged to consider whether nutrient management strategies can slow the progression of acidification and deoxygenation and their impact on coastal habitats (Kelly et al. 2011, Strong et al. 2014, Chan et al. 2016). Globally, wastewater discharge, 80% of which is untreated (WWAP 2017), represents a significant pathway of nutrient enrichment and eutrophication of coastal waters. However, the relative impact of these inputs compared to global change on N and C biogeochemical cycling is poorly characterized (Kelly et al. 2011, Strong et al. 2014), particularly in EBUS. In this study, we document that wastewater nutrient inputs have an immediate, local effect on nutrient stoichiometry, elevating ammonium and nitrite concentrations and increasing dissolved nitrogen: phosphorus ratios, as well as increasing rates of nitrification within the plume. We did not observe a consistent, near plume effect in nitrate assimilation, primary production, chlorophyll *a*, respiration, or DO, suggesting any potential impact from wastewater on these processes is moderated by regional factors, notably mixing of water. This suggests that further study of implications of these changes on the SCB lower trophic ecosystem through ocean numerical modeling studies is warranted, given the difficulty in disentangling local versus regional versus global drivers through observations alone.

Anthropogenic nutrient inputs impact the biogeochemical cycling of nitrogen in the immediate, local vicinity of outfalls

The doubling of coastal ocean annual nitrogen loads from wastewater outfalls (Howard et al. 2014) has important implications for nitrogen cycling in the nearshore. Wastewater nitrogen appears to be altering the composition of the N pool within the plumes; ammonium and nitrite concentrations are elevated in the nearfield regions compared to farfield regions (Figure 3). The high concentrations of ammonium in the nearfield and the relatively small percentage of labeled ammonium added to these samples during the incubation experiments (less than 1% spike) may have resulted in an underestimation of nitrification in the nearfield

1 samples. Therefore, the differences in nitrification rates in the nearfield compared to the
2 farfield may be greater than what is described here.

3 The N:P ratio in coastal waters also appears to be altered by the presence of wastewater
4 plumes. The ratio of N:P is a nearly constant 16:1 throughout the world's oceans, in both
5 phytoplankton biomass and in dissolved nutrient pools (Redfield 1958), and the farfield stations
6 adhere closely to this ratio (Figure 4). However, the nearfield stations have elevated N:P ratios,
7 which can be attributed to the relatively low concentrations of P compared to N in wastewater
8 (Table 2, effluent N:P ~115:1). This increase in P-limitation near outfalls may have important
9 implications for the phytoplankton community composition near these discharges (Grosse et al.
10 2017, Moreno and Martiny 2018, Fagan et al. 2019). This could be particularly problematic for
11 harmful algal bloom species (HABs), as P-limitation has been linked to increased toxin
12 production in *Pseudo-nitzschia* (Fehling et al. 2004), a common HABs species in the SCB
13 (Schnetzer et al. 2007b).

14 Nitrification of ammonium to nitrate has been found to play an important role in coastal
15 ocean nitrogen cycling (Ward 1987, 2005) and can support a significant fraction of productivity
16 in surface waters (Wankel et al. 2007, Santoro et al. 2010). Offshore (farfield) rates were
17 consistent with those measured in similar locations in the Southern California Bight (Ward
18 1987) and coastal locations in Monterey Bay, California (Ward 2005, Smith et al. 2014), but
19 slightly lower than those measured within the California Current (Santoro et al. 2010). The rate
20 of nitrification is light inhibited and related to ammonium concentration (Ward 2008). Our
21 results are consistent with this, where nitrification rates show positive correlations with water
22 column N species and negative correlations with DO, temperature (Spearman rank analysis,
23 Table 3). Random forest regressions explained a relatively low percent of the variance for
24 nitrification rates, 20% (Figure SI.10). Phosphate and station type, were most predictive,
25 followed by temperature, nitrate and dissolved oxygen, likely related to the fact that nitrifying
26 bacteria are typically light inhibited and thus more abundant below the eutrophic zone, where
27 water temperatures were colder and dissolved oxygen is lower (Ward 1987, 2005, Santoro et al.
28 2010, Smith et al. 2014). The low percentage of the variability explained by the random forest

models suggests that there were other factors which affect the nitrification rates, such as the composition of the bacterial community (Ward 2005).

Wastewater N is predominantly ammonium and is discharged at depth, rising in a buoyant plume and generally trapped below the mixed layer (Figure 3) (Nezlin et al. 2020). Because wastewater ammonium is discharged at depth below the photic zone, wastewater ammonium was expected to be rapidly nitrified. Indeed, elevated nitrite concentrations and higher nitrification rates were associated with OCSD's effluent plume (McLaughlin et al. 2017), and effluent discharges in other coastal regions have seen similarly elevated nitrification rates in sediments near outfalls (Axelrad et al. 1981, Nowicki 1994). Furthermore, the OCSD diversion study was able to track changes in nitrification rates when the plume is "turned-off" relative to "turned-on" and results suggested that wastewater ammonium was nitrified on relatively short time scales; hours to days (McLaughlin et al. 2017). Thus, the contribution of nitrate from the nitrification of wastewater effluent has the potential to support significant productivity in coastal areas. Ammonium concentrations were elevated in nearfield stations relative to farfield stations, particularly at the depths associated with the plume (Figure 3). These high ammonium concentrations are associated with increased nitrification rates, both directly over the outfall and in "older" plume, suggesting a local impact on N cycling from wastewater effluent discharges. Generally, LACSD's nitrification rates were higher than OCSD's, particularly below the thermocline, which is consistent with the higher concentrations of ammonium in effluent (Figure SI.9). However, OCSD had much greater variability in nitrification rates near its outfall compared to LACSD, with relatively high nitrification rates within the chlorophyll maximum and within the mixed layer, as well as the highest recorded nitrification rate in a bottom sample during Spring 2015, demonstrating the variability present in the rates both within a site and across the region. Concentrations of nitrite, likely from oxidation of ammonium, were elevated within the plume over both outfalls (Figure 3). Nitrate concentrations were not significantly elevated in the nearfield relative to farfield stations; however, the concentrations of nitrate were 2-3 times higher than ammonium and 10 times higher than nitrite, thus the additional contribution from nitrification if diluted over a larger area may not have been distinguishable from local heterogeneity in concentrations.

1 Nitrification rates were not higher in the “fresh” plume compared to “older” plume stations,
2 suggesting that the time-scales of nitrification of plume ammonium were on the order of days
3 and that the elevation in nitrification rates encompasses, at minimum, plume areas as defined
4 by this study (i.e., detectable by CDOM).

5
6 ***Regional factors play a more important role in nitrate assimilation compared to localized***
7 ***impacts of wastewater plume.***

8 Nitrate assimilation (incorporation of nitrate into the biomass) was not directly
9 measured in this study; however, stable isotopes were employed as tracers of this process in
10 the water column. While the relative enrichments in $\delta^{15}\text{N}_{\text{NO}_2+\text{NO}_3}$ and $\delta^{18}\text{O}_{\text{NO}_3}$ often fell along a
11 line with a slope of 1 (Figure 5C, Figure SI.5), particularly during the Spring 2016 event, the low
12 surface values in $\delta^{15}\text{N}_{\text{NO}_2+\text{NO}_3}$ during the first three sampling periods resulted in poor or negative
13 correlation between $\delta^{15}\text{N}_{\text{NO}_2+\text{NO}_3}$ and $\delta^{18}\text{O}_{\text{NO}_3}$ for some stations. A linear relationship between
14 $\delta^{15}\text{N}_{\text{NO}_2+\text{NO}_3}$ and $\delta^{18}\text{O}_{\text{NO}_3}$ with a slope of 1 would be predicted if phytoplankton assimilation or
15 denitrification were the dominant processes controlling the isotopic composition of nitrate
16 (Granger et al. 2004). However, because concentrations of oxygen were relatively high (always
17 greater than 2 mg L^{-1}), denitrification is not likely to be a significant process in these waters and
18 the isotope affect is likely to be attributed to assimilation (Wankel et al. 2007).

19 Nitrate assimilation was not significantly different in nearfield areas versus farfield
20 areas, but had clear seasonal patterns, suggesting regional mixing and dilution of wastewater N
21 likely spreads the impact on assimilation over a much wider area thereby creating a potential
22 temporal lag in effect. During upwelling periods, particularly during the Spring of 2016, the
23 effect of nitrate assimilation on the isotopic composition of the dissolved nitrate pool is evident
24 from the measurements of $\delta^{18}\text{O}_{\text{NO}_3}$ and $\delta^{15}\text{N}_{\text{NO}_2+\text{NO}_3}$ falling along a 1:1 line (Figure 5C, Figure
25 SI.5). However, during the Summer sampling periods, the isotope effect from assimilation of
26 “new” nitrate from upwelling is diluted and the relationship between the two isotopes appears
27 more influenced by nitrification. In Monterey Bay, in northern California, nitrification of
28 “natural” ammonium from regenerated organic matter was found to contribute ~30% of nitrate
29 based primary production (Wankel et al. 2007). The isotopic composition of dissolved nitrate at

all stations increased with nitrate concentration and the fraction of nitrate in the DIN pool. This is consistent with nitrification as a significant driver defining the composition of the DIN pool and the isotopic composition thereof, region-wide (Sugimoto et al. 2009, McLaughlin et al. 2017). However, because nitrification is largely happening below the euphotic zone, the importance of this source for regional primary productivity will be directly related to physical mixing in the region. Time scales of when this subsurface nitrate source mixes into the surface waters could result in impacts of this source in the farfield regions and not necessarily near the discharge location.

Impacts of anthropogenic nutrient inputs on the biogeochemical cycling of carbon and oxygen are regional in scale.

Regional factors such as upwelling and Pacific Basin-scale changes in circulation have been shown to be the primary drivers for the concentrations of chlorophyll biomass and the depth of the chlorophyll maximum layer (Mantyla et al. 2008, Nezlin et al. 2012, Nezlin et al. 2018). This work highlights the importance of regional-scale influences on carbon and oxygen cycling. In this study, no statistically significant differences in primary productivity and respiration were found in nearfield areas versus farfield (Figure 7). This is consistent with an investigation of pH and aragonite saturation state during the same time period as this study, which found no significant differences between these parameters on the continental shelf (near anthropogenic discharges) compared to offshore of these influences (McLaughlin et al. 2018). While there were some regional differences in chlorophyll *a* and dissolved oxygen, they were not clearly linked to proximity to the wastewater plume, although the highest recorded chlorophyll fluorescence values were in nearfield stations (Figure 2, Table 3). The alteration of the N:P ratios in nearfield regions could impact phytoplankton community productivity as noted above (Grosse et al. 2017, Moreno and Martiny 2018, Fagan et al. 2019), resulting in a dilution of the impact of increased N over a larger area. Furthermore, we saw evidence of seasonal upwelling bringing increased chlorophyll biomass and intrusions of deep, cold waters that are low in dissolved oxygen into surface waters; impacting both nearfield and farfield regions. This supports the hypothesis that regional mixing of water masses dilutes the impact of wastewater

1 N on the coastal environment, potentially enhanced by outfall diffuser systems which discharge
2 effluent over large areas, spreading the effect on primary production and respiration over
3 larger areas, and by extension carbon and oxygen cycling in the SCB (Mantyla et al. 2008, Nezhlin
4 et al. 2012, Nezhlin et al. 2018).

5 Random forest regression characterized a low percent of variance for both primary
6 production and respiration (30% and 18%, respectively Figure SI.11), thus the primary drivers
7 for variability in these processes were either not well accounted for in the observed parameters
8 or the relationships between factors are diluted regionally. Season was the most predictive
9 variable of primary production in random forest analysis, indicating the importance of regional
10 variables on primary productivity, as the SCB is subject to seasonal upwelling. This is shown in
11 the seasonal differences in temperature, salinity and chlorophyll *a* during the study (Figure 2).
12 Station type was not very predictive for either primary production or respiration, suggesting
13 any impact of the wastewater plume is diluted across the region. This dilution effect is also
14 apparent in the isotopic signature of the assimilation of “new” nitrate on $\delta^{15}\text{N}_{\text{NO}_2+\text{NO}_3}$ is also
15 mixed throughout the study area, particularly during Summer, stratified, periods (Figure 5C).
16 Furthermore, concentrations of suspended particulate matter (carbon, nitrogen and
17 phosphorus) and nutrient ratios within that suspended matter were not significantly different
18 in the nearfield versus the farfield (Figures 4 and 5). This decoupling of the presence of the
19 wastewater plume, and its associated nutrients, from primary production, suspended organic
20 matter, and respiration can be explained by regional dilution of effluent nitrogen due to water
21 mass mixing. Both LACSD and OCSD outfalls have multiport diffusers to disperse and increase
22 dilution of the plume over a large area to minimize immediate local impacts of the discharge on
23 the coastal ocean environment (Koh and Brooks 1975). The relative buoyancy of the plume to
24 local seawater traps the plume in the subsurface near the base of the euphotic zone where
25 they could be utilized by primary producers, but the impact is designed to be diluted over a
26 larger area dictated by the local hydrodynamics of plume mixing as well as seasonal, basin-scale
27 changes in currents and ocean state. Given that no difference was observed in primary
28 production and respiration in plume affected areas relative to farfield areas, it is likely that

1 effect of effluent nutrients on these processes are either diluted throughout the region into
2 farfield areas or is too small to detect.

3 Isotopic signatures of particulate matter ($\delta^{15}\text{N}_{\text{PM}}$ and $\delta^{13}\text{C}_{\text{PM}}$) were also not significantly
4 different across stations (Figure 5). The isotopic composition of nitrogen in suspended material
5 ($\delta^{15}\text{N}_{\text{PM}}$) is slightly lower than dissolved nitrate in the water column ($\delta^{15}\text{N}_{\text{NO}_2+\text{NO}_3}$) indicating the
6 presence of a small isotopic discrimination associated with uptake of nitrate into the biomass
7 (Figure 5H) (Ostrom et al. 1997). Furthermore, $\delta^{15}\text{N}_{\text{PM}}$ increased with chlorophyll fluorescence
8 (Figure 5I). The lighter isotope is preferentially utilized by phytoplankton and, as N becomes
9 limiting, this isotopic discrimination becomes less and less until the isotopic composition of the
10 biomass is the same as that of the N being utilized (Ostrom et al. 1997). $\delta^{15}\text{N}_{\text{PM}}$ values typically
11 asymptote to values between 5 and 8 ‰ with increasing chlorophyll, although the asymptote
12 for plume areas versus farfield areas were not significantly different, further indicating that
13 nitrogen sourcing for primary production and associated chlorophyll *a* biomass, has a more
14 regional signal rather than attributable to a specific source.

15 There were no consistent spatial or seasonal patterns in the isotopic signatures of
16 nitrogen and carbon in particulate matter (Figure 6); however, $\delta^{13}\text{C}_{\text{PM}}$ increased with
17 chlorophyll fluorescence in the water column (Figure 5F). Using chlorophyll *a* as a proxy for
18 phytoplankton biomass, an increase in $\delta^{13}\text{C}_{\text{PM}}$ with biomass is consistent with lowering of
19 dissolved inorganic carbon and dissolved carbon dioxide (Ostrom et al. 1997). This has
20 important implications for regional variability in acidification. Nutrient enrichment of coastal
21 waters has been linked to impacts on the aragonite saturation state, inducing waters into
22 undersaturated conditions when they otherwise might not have been (Cai et al. 2011, Wallace
23 et al. 2014, Rheuban et al. 2019). Regionally, the SCB is exposed to waters with aragonite
24 saturations states below thresholds thought to be important for marine calcifiers (McLaughlin et
25 al. 2018), and further investigation into potential enhancement of acidification associated with
26 increased primary production is therefore warranted.

The failings of a “reference-area” approach to document impacts of point sources on nutrient and carbon cycling.

The study design was based upon the hypothesis that areas near wastewater outfalls would be more impacted from nutrient discharges than areas spatially distant from the outfalls. Results suggest that such a concept is only true for nitrification, which occurs at depths directly associated with detectable plume. For primary production, assimilation, and respiration, an immediate, local effect was not observed. While a slight lag in the timing (and thus distance) of elevated primary production and chlorophyll *a* from wastewater N discharged by ocean outfalls at depth was expected, the observations suggest that levels of advection, stirring, and eventual mixing in the region were sufficient to transport anthropogenic nutrients to presumed “minimally disturbed” reference areas in the farfield. Thus, the concept of a “reference area” (Nezlin et al., 2020) as implemented here in the SCB is flawed for nutrient impacts on these processes. This is supported by numerical ocean model simulations from the Regional Ocean Modeling System (ROMS, www.myroms.org; (Shchepetkin and McWilliams 2005)) run in particle tracking mode to track lagrangian flow of “plume particles” (Figure 8). When particles were released from the outfalls, they were transported to farfield areas used for this study on timescales of weeks to months, suggesting that wastewater N is mixed over larger regional scales before contributing significantly to primary production. In such cases, impacts of anthropogenic nutrients on primary production, related elevation in respiration, and impacts on carbon cycling/acidification, are not easily deciphered with observational data alone. Thus, the monitoring scheme to assess nutrient impacts should be reevaluated to include modeling approaches that can account for the complexity of mixing and farfield transport in the region.

Conclusion

In this study, we found that wastewater nutrient inputs have an immediate, local effect on nutrient stoichiometry and nitrogen concentrations and elevated rates of nitrification within the plume. Impact of wastewater plumes on nitrate assimilation, primary production, chlorophyll *a*, respiration, and DO was moderated by regional mixing of water masses. This lends strong support for further study of local anthropogenic forcing through ocean numerical

modeling studies, given the difficulty in disentangling local to global scale drivers through observations alone (Chan et al. 2016). While observational studies such as this are costly, they provide key data needed to evaluate ocean numerical models. These data should not only include state variables, which can be used to characterize the uncertainty in model output (is the model getting the right answers), but also rate variables, which can be used to determine if the model configuration accurately represents the underlying biogeochemical processes creating that output (is the model getting the right answers for the right reasons).

References

- Anderson, C. R., M. A. Brzezinski, L. Washburn, and R. Kudela. 2006. Circulation and environmental conditions during a toxigenic *pseudo-nitzschia australis* bloom in the santa barbara channel, california. *Marine Ecology Progress Series* **327**:119-133.
- Axelrad, D., G. Poore, G. Arnott, J. Bauld, V. Brown, R. Edwards, and N. Hickman. 1981. The effects of treated sewage discharge on the biota of port phillip bay, victoria, australia. Pages 279-306 *Estuaries and nutrients*. Springer.
- Boesch, D. F. 2019. Barriers and bridges in abating coastal eutrophication. *Frontiers in Marine Science* **6**:123.
- Bograd, S. J., C. G. Castro, E. Di Lorenzo, D. M. Palacios, H. Bailey, W. Gilly, and F. P. Chavez. 2008. Oxygen declines and the shoaling of the hypoxic boundary in the california current. *Geophys. Res. Lett.* **35**:L12607
- Booth, J. A. T., C. B. Woodson, M. Sutula, F. Micheli, S. B. Weisberg, S. J. Bograd, A. Steele, J. Schoen, and L. B. Crowder. 2014. Patterns and potential drivers of declining oxygen content along the southern california coast. *Limnology and Oceanography* **59**:1127-1138.
- Borges, A. V. and N. Gypens. 2010. Carbonate chemistry in the coastal zone responds more strongly to eutrophication than to ocean acidification. *Limnology and Oceanography* **55**:346-353.
- Breiman, L. 2001. Random forests. *Machine learning* **45**:5-32.

- 1 Breitburg, D., L. A. Levin, A. Oschlies, M. Grégoire, F. P. Chavez, D. J. Conley, V. Garçon, D.
2 Gilbert, D. Gutiérrez, and K. Isensee. 2018. Declining oxygen in the global ocean and
3 coastal waters. *Science* **359**.
- 4 Brzezinski, M. A. and L. Washburn. 2011. Phytoplankton primary productivity in the santa
5 barbara channel: Effects of wind-driven upwelling and mesoscale eddies. *Journal of*
6 *Geophysical Research: Oceans* **116**.
- 7 Cai, W. J., X. P. Hu, W. J. Huang, M. C. Murrell, J. C. Lehrter, S. E. Lohrenz, W. C. Chou, W. D.
8 Zhai, J. T. Hollibaugh, Y. C. Wang, P. S. Zhao, X. H. Guo, K. Gundersen, M. H. Dai, and G.
9 C. Gong. 2011. Acidification of subsurface coastal waters enhanced by eutrophication.
10 *Nature Geoscience* **4**:766-770.
- 11 Capone, D. G. and D. A. Hutchins. 2013. Microbial biogeochemistry of coastal upwelling regimes
12 in a changing ocean. *Nature Geoscience* **6**:711-717.
- 13 Casciotti, K. L., D. M. Sigman, M. G. Hastings, J. K. Bohlke, and A. Hilkert. 2002. Measurement of
14 the oxygen isotopic composition of nitrate in seawater and freshwater using the
15 denitrifier method. *Analytical Chemistry* **74**:4905-4912.
- 16 Chan, F., A. B. Boehm, J. A. Barth, E. A. Chornesky, A. G. Dickson, R. A. Feely, B. Hales, T. M. Hill,
17 G. Hofmann, D. Ianson, T. Klinger, J. Largier, J. Newton, T. F. Pedersen, G. N. Somero, M.
18 Sutula, W. W. Wakefield, G. G. Waldbusser, S. B. Weisberg, and E. A. Whiteman. 2016.
19 The west coast ocean acidification and hypoxia science panel: Major findings,
20 recommendations, and actions., Oakland, California, USA.
- 21 Chavez, F. P. and M. Messié. 2009. A comparison of eastern boundary upwelling ecosystems.
22 *Progress in Oceanography* **83**:80-96.
- 23 Cullen, J. and R. Eppley. 1981. Chlorophyll maximum layers of the southern-california bight and
24 possible mechanisms of their formation and maintenance. *Oceanologica Acta* **4**:23-32.
- 25 Cutler, D. R., T. C. Edwards, K. H. Beard, A. Cutler, K. T. Hess, J. Gibson, and J. J. Lawler. 2007.
26 Random forests for classification in ecology. *Ecology* **88**:2783-2792.
- 27 Dauhajre, D. P., J. C. McWilliams, and L. Renault. 2019. Nearshore lagrangian connectivity:
28 Submesoscale influence and resolution sensitivity. *Journal of Geophysical Research:*
29 *Oceans* **124**:5180-5204.

- 1 Diaz, R.J. and Rosenberg, R., 2008. Spreading dead zones and consequences for marine
2 ecosystems. *science*, 321(5891), pp.926-929.
- 3 Deutsch, C., H. Frenzel, J. C. McWilliams, L. Renault, F. Kessouri, E. Howard, J.-H. Liang, D.
4 Bianchi, and S. Yang. in review. Biogeochemical variability in the california current
5 system. <https://doi.org/10.1101/2020.02.10.942565>.
- 6 Deutsch, C., N. Gruber, R. M. Key, J. L. Sarmiento, and A. Ganachaud. 2001. Denitrification and
7 n-2 fixation in the pacific ocean. *Global Biogeochemical Cycles* **15**:483-506.
- 8 Eppley, R. W. 1992. Chlorophyll, photosynthesis and new production in the southern california
9 bight. *Progress in oceanography* **30**:117-150.
- 10 Fagan, A. J., A. R. Moreno, and A. C. Martiny. 2019. Role of enso conditions on particulate
11 organic matter concentrations and elemental ratios in the southern california bight.
12 *Frontiers in Marine Science* **6**:386.
- 13 Fehling, J., K. Davidson, C. J. Bolch, and S. S. Bates. 2004. Growth and domoic acid production by
14 pseudo-nitzschia seriata (bacillariophyceae) under phosphate and silicate limitation 1.
15 *Journal of Phycology* **40**:674-683.
- 16 Fennel, K. and J. M. Testa. 2019. Biogeochemical controls on coastal hypoxia. *Annual Review of*
17 *Marine Science* **11**:105-130.
- 18 Glibert, P. M., J. Harrison, C. Heil, and S. Seitzinger. 2006. Escalating worldwide use of urea - a
19 global change contributing to coastal eutrophication. *Biogeochemistry* **77**:441-463.
- 20 Goldman, J. C., D. A. Caron, and M. R. Dennett. 1987. Regulation of gross growth efficiency and
21 ammonium regeneration in bacteria by substrate c-n ratio. *Limnology and*
22 *Oceanography* **32**:1239-1252.
- 23 Grosse, J., A. Burson, M. Stomp, J. Huisman, and H. T. Boschker. 2017. From ecological
24 stoichiometry to biochemical composition: Variation in n and p supply alters key
25 biosynthetic rates in marine phytoplankton. *Frontiers in microbiology* **8**:1299.
- 26 Gruber, N. and J. L. Sarmiento. 1997. Global patterns of marine nitrogen fixation and
27 denitrification. *Global Biogeochemical Cycles* **11**:235-266.
- 28 Henriksen, K. 1988. Nitrification in estuarine and coastal marine sediments. *Nitrogen cycling in*
29 *coastal marine environments*.

- 1 Holmes, R. M., A. Aminot, R. Kerouel, B. A. Hooker, and B. J. Peterson. 1999. A simple and
2 precise method for measuring ammonium in marine and freshwater ecosystems.
3 Canadian Journal of Fisheries and Aquatic Sciences **56**:1801-1808.
- 4 Howard, M. D. A., M. Sutula, D. A. Caron, Y. Chao, J. D. Farrara, H. Frenzel, B. Jones, G.
5 Robertson, K. McLaughlin, and A. Sengupta. 2014. Anthropogenic nutrient sources rival
6 natural sources on small scales in the coastal waters of the southern california bight.
7 Limnology and Oceanography **59**:285-297.
- 8 Howarth, R. W., A. Sharpley, and D. Walker. 2002. Sources of nutrient pollution to coastal
9 waters in the united states: Implications for achieving coastal water quality goals.
10 Estuaries **25**:656-676.
- 11 Kelley, D. and C. Richards. 2017. Oce: Analysis of oceanographic data. R package version 0.9-21.
12 Retrieved from <https://CRAN.R-project.org/package=oce>.
- 13 Kelly, R. P., M. Foley, W. Fisher, R. Feely, B. Halpern, G. Waldbusser, and M. Caldwell. 2011.
14 Mitigating local causes of ocean acidification with existing laws. Science **332**:1036-1037.
- 15 Koch, S. E., M. desJardins, and P. J. Kocin. 1983. An interactive Barnes objective map analysis
16 scheme for use with satellite and conventional data. Journal of Applied Meteorology
17 and Climatology **22**:1487-1503.
- 18 Koh, R. C. and N. H. Brooks. 1975. Fluid mechanics of waste-water disposal in the ocean. Annual
19 Review of Fluid Mechanics **7**:187-211.
- 20 Mantyla, A. W., S. J. Bograd, and E. L. Venrick. 2008. Patterns and controls of chlorophyll-a and
21 primary productivity cycles in the southern california bight. Journal of Marine Systems
22 **73**:48-60.
- 23 McLaughlin, K., N. P. Nezlin, M. D. Howard, C. D. Beck, R. M. Kudela, M. J. Mengel, and G. L.
24 Robertson. 2017. Rapid nitrification of wastewater ammonium near coastal ocean
25 outfalls, southern california, USA. Estuarine, Coastal and Shelf Science **186**:263-275.
- 26 McLaughlin, K., N. P. Nezlin, S. B. Weisberg, A. G. Dickson, J. A. T. Booth, C. L. Cash, A. Feit, J. R.
27 Gully, M. D. Howard, and S. Johnson. 2018. Seasonal patterns in aragonite saturation
28 state on the southern california continental shelf. Continental Shelf Research **167**:77-86.

- 1 Moreno, A. R. and A. C. Martiny. 2018. Ecological stoichiometry of ocean plankton. Annual
2 Review of Marine Science **10**:43-69.
- 3 Nezlin, N., M. A. Sutula, R. P. Stumpf, and A. Sengupta. 2012. Phytoplankton blooms detected
4 by seawifs along the central and southern california coast. Journal of Geophysical
5 Research **117**:C07004.
- 6 Nezlin, N. P., C. Beegan, A. Feit, J. R. Gully, A. Latker, K. McLaughlin, M. J. Mengel, G. L.
7 Robertson, A. Steele, and S. B. Weisberg. 2020. Colored dissolved organic matter (cdom)
8 as a tracer of effluent plumes in the coastal ocean. Regional Studies in Marine Science
9 **35**:101163.
- 10 Nezlin, N. P., K. McLaughlin, J. A. T. Booth, C. L. Cash, D. W. Diehl, K. A. Davis, A. Feit, R.
11 Goericke, J. R. Gully, and M. D. Howard. 2018. Spatial and temporal patterns of
12 chlorophyll concentration in the southern california bight. Journal of Geophysical
13 Research: Oceans **123**:231-245.
- 14 Nowicki, B. L. 1994. The effect of temperature, oxygen, salinity, and nutrient enrichment on
15 estuarine denitrification rates measured with a modified nitrogen gas flux technique.
16 Estuarine, Coastal and Shelf Science **38**:137-156.
- 17 Ostrom, N. E., S. A. Macko, D. Deibel, and R. J. Thompson. 1997. Seasonal variation in the stable
18 carbon and nitrogen isotope biogeochemistry of a coastal cold ocean environment.
19 Geochimica et Cosmochimica Acta **61**:2929-2942.
- 20 Patton, C. and J. R. Kryskalla. 2003. Methods of analysis by the u.S. Geological survey national
21 water quality laboratory—evaluation of alkaline persulfate digestion as an alternative to
22 kjeldahl digestion for determination of total and dissolved nitrogen and phosphorus in
23 water, water-resources investigations report 03–4174. U.S. Department of the Interior,
24 U.S. Geological Survey, Denver, CO.
- 25 Powley, H. R., H. H. Dürr, A. T. Lima, M. D. Krom, and P. Van Cappellen. 2016. Direct discharges
26 of domestic wastewater are a major source of phosphorus and nitrogen to the
27 mediterranean sea. Environmental Science & Technology **50**:8722-8730.

- 1 Prasad, A. M., L. R. Iverson, and A. Liaw. 2006. Newer classification and regression tree
2 techniques: Bagging and random forests for ecological prediction. *Ecosystems* **9**:181-
3 199.
- 4 Provoost, P., S. Van Heuven, K. Soetaert, R. Laane, and J. Middelburg. 2010. Seasonal and long-
5 term changes in ph in the dutch coastal zone. *Biogeosciences* **7**:3869.
- 6 Rabalais, N. N., W.-J. Cai, J. Carstensen, D. J. Conley, B. Fry, X. Hu, Z. Quinones-Rivera, R.
7 Rosenberg, C. P. Slomp, and R. E. Turner. 2014. Eutrophication-driven deoxygenation in
8 the coastal ocean. *Oceanography* **27**:172-183.
- 9 Redfield, A. C. 1958. The biological control of chemical factors in the environment. *American*
10 *Scientist* **46**:205-221.
- 11 Rheuban, J. E., S. C. Doney, D. C. McCorkle, and R. W. Jakuba. 2019. Quantifying the effects of
12 nutrient enrichment and freshwater mixing on coastal ocean acidification. *Journal of*
13 *Geophysical Research: Oceans*.
- 14 Roberts, P. J., H. J. Salas, F. M. Reiff, M. Libhaber, A. Labbe, and J. C. Thomson. 2010. Marine
15 wastewater outfalls and treatment systems. IWA publishing.
- 16 Rogowski, P., E. Terrill, M. P. Otero, L. Hazard, and W. Middleton. 2012. Mapping ocean outfall
17 plumes and their mixing using autonomous underwater vehicles. *Journal of Geophysical*
18 *Research-Oceans* **117** 1-12.
- 19 Rogowski, P., E. Terrill, M. P. Otero, L. Hazard, and W. Middleton. 2013. Ocean outfall plume
20 characterization using an autonomous underwater vehicle. *Water Science and*
21 *Technology* **67**:925-933.
- 22 Santoro, A. E., K. L. Casciotti, and C. A. Francis. 2010. Activity, abundance and diversity of
23 nitrifying archaea and bacteria in the central california current. *Environmental*
24 *Microbiology* **12**:1989-2006.
- 25 Schnetzer, A., B. H. Jones, R. A. Schaffner, I. Cetinic, E. Fitzpatrick, P. E. Miller, E. L. Seubert, and
26 D. A. Caron. 2013. Coastal upwelling linked to toxic pseudo-nitzschia australis blooms in
27 los angeles coastal waters, 20052007. *Journal of Plankton Research* **35**:1080-1092.
- 28 Schnetzer, A., P. E. Miller, R. A. Schaffner, B. A. Stauffer, B. H. Jones, S. B. Weisberg, P. M.
29 DiGiacomo, W. M. Berelson, and D. A. Caron. 2007a. Blooms of pseudo-nitzschia and

domoic acid in the san pedro channel and los angeles harbor areas of the southern
california bight, 2003-2004. *Harmful Algae* **6**:372-387.

Schnetzer, A., P. E. Miller, R. A. Schaffner, B. A. Stauffer, B. H. Jones, S. B. Weisberg, P. M.
DiGiacomo, W. M. Berelson, and D. A. Caron. 2007b. Blooms of pseudo-nitzschia and
domoic acid in the san pedro channel and los angeles harbor areas of the southern
california bight, 2003–2004. *Harmful algae* **6**:372-387.

Shchepetkin, A. F. and J. C. McWilliams. 2005. The regional oceanic modeling system (roms): A
split-explicit, free-surface, topography-following-coordinate oceanic model. *Ocean
modelling* **9**:347-404.

Sigman, D. M., J. Granger, P. J. DiFiore, M. M. Lehmann, R. Ho, G. Cane, and A. van Geen. 2005.
Coupled nitrogen and oxygen isotope measurements of nitrate along the eastern north
pacific margin. *Global Biogeochemical Cycles* **19**.

Smith, J. M., K. L. Casciotti, F. P. Chavez, and C. A. Francis. 2014. Differential contributions of
archaeal ammonia oxidizer ecotypes to nitrification in coastal surface waters. *The ISME
journal* **8**:1704.

Smith, R., R. Eppley, and K. Baker. 1982. Correlation of primary production as measured aboard
ship in southern california coastal waters and as estimated from satellite chlorophyll
images. *Marine Biology* **66**:281-288.

Smith, J.; Connell, P.; Evans, R. H.; Gellene, A. G.; Howard, M. D. A.; Jones, B. H.; Kaveggia, S.;
Palmer, L.; Schnetzer, A.; Seegers, B. N.; Seubert, E. L.; Tatters, A. O.; Caron, D. A., A
decade and a half of *Pseudo-nitzschia* spp. and domoic acid along the coast of southern
California. *Harmful Algae* **2018**, *79*, 87-104.

Strong, A. L., K. J. Kroeker, L. T. Teneva, L. A. Mease, and R. P. Kelly. 2014. Ocean acidification
2.0: Managing our changing coastal ocean chemistry. *Bioscience* **64**:581-592.

Sugimoto, R., A. Kasai, T. Miyajima, and K. Fujita. 2009. Controlling factors of seasonal variation
in the nitrogen isotope ratio of nitrate in a eutrophic coastal environment. *Estuarine
Coastal and Shelf Science* **85**:231-240.

- 1 Sunda, W. G. and W.-J. Cai. 2012. Eutrophication induced co₂-acidification of subsurface coastal
2 waters: Interactive effects of temperature, salinity, and atmospheric p co₂.
3 Environmental Science & Technology **46**:10651-10659.
- 4 Sutton, A., R. Wanninkhof, C. Sabine, R. Feely, M. Cronin, and R. Weller. 2017. Variability and
5 trends in surface seawater pco₂ and co₂ flux in the pacific ocean. Geophysical Research
6 Letters **44**:5627-5636.
- 7 Sutula, M., A. Sengupta, M. Ho, F. Kessouri, K. McLaughlin, K. McCune, and D. Bianchi. 2020.
8 Southern california bight rivers, wastewater effluents and atmospheric data.
9 <https://doi.org/10.5281/zenodo.3981643>.
- 10 Thomas, W. H., D. L. Seibert, and A. N. Dodson. 1974. Phytoplankton enrichment experiments
11 and bioassays in natural coastal sea water and in sewage outfall receiving waters off
12 southern california. Estuarine and Coastal Marine Science **2**:191-206.
- 13 Valiela, I., C. Owens, E. Elmstrom, and J. Lloret. 2016. Eutrophication of cape cod estuaries:
14 Effect of decadal changes in global-driven atmospheric and local-scale wastewater
15 nutrient loads. Marine Pollution Bulletin **110**:309-315.
- 16 Waldbusser, G. G. 2011. The causes of acidification in chesapeake bay and consequences to
17 oyster shell growth and dissolution. Pages 559-560 in Journal of Shellfish Research. NATL
18 SHELLFISHERIES ASSOC C/O DR. SANDRA E. SHUMWAY, UNIV CONNECTICUT, 1080
- 19 Waldbusser, G. G., H. Bergschneider, and M. A. Green. 2010. Size-dependent ph effect on
20 calcification in post-larval hard clam mercenaria spp. Marine Ecology Progress Series
21 **417**:171-182.
- 22 Wallace, R. B., H. Baumann, J. S. Grear, R. C. Aller, and C. J. Gobler. 2014. Coastal ocean
23 acidification: The other eutrophication problem. Estuarine, Coastal and Shelf Science
24 **148**:1-13.
- 25 Wankel, S. D., C. Kendall, C. A. Francis, and A. Paytan. 2006. Nitrogen sources and cycling in the
26 san francisco bay estuary: A nitrate dual isotopic composition approach. Limnology and
27 Oceanography **51**:1654-1664.

1 Wankel, S. D., C. Kendall, J. T. Pennington, F. P. Chavez, and A. Paytan. 2007. Nitrification in the
2 euphotic zone as evidenced by nitrate dual isotopic composition: Observations from
3 monterey bay, california. *Global Biogeochemical Cycles* **21**.
4 Ward, B. B. 1987. Nitrogen transformations in the southern california bight. *Deep-Sea Research*
5 **34**:785-805.
6 Ward, B. B. 2005. Temporal variability in nitrification rates and related biogeochemical factors
7 in monterey bay, california, USA. *Marine Ecology Progress Series* **292**:97-109.
8 Ward, B. B. 2008. Nitrification in marine systems.
9 Wood, I. R., R. G. Bell, and D. L. Wilkinson. 1993. Ocean disposal of wastewater. *World*
10 *Scientific*.
11
12

Contributions

Karen McLaughlin was the co-lead on this project with Meredith Howard. McLaughlin contributed to study design, led the nutrient and stable isotope analysis and nitrification rates study, conducted the data analysis and drafted the final report.

Meredith D.A. Howard was the co-lead on the project with Karen McLaughlin. She contributed to study design, managed project budget, coordinated the field work and led the primary production and respiration portions of the study. She contributed to primary production and respiration sections of the report and reviewed the final draft.

George Robertson coordinated field sampling with the Sanitation Districts, contributed to study design, reviewed data analysis plan and preliminary data, and reviewed the manuscript on behalf of management agencies.

Carly D.A. Beck was the lead research technician on the project. She contributed to study design, managed field staff in the field and coordinated data collection and quality assurance and reviewed the final report.

Minna Ho is a partner on the modeling effort. She provided the particle tracking model output and interpretation of the observational data.

Fayçal Kessouri is the lead modeler working on nutrient impacts on coastal environments. Kessouri engineered the ROMS model used for particle tracking model output and interpretation of the observational data.

Nikolay P. Nezlin contributed data analysis for the nitrification study and analysis of water column profiles.

Martha Sutula is the Principal Investigator of the Biogeochemistry Department at SCCWRP, she contributed project management, study design, and drafted portions of the final report.

Stephen B. Weisberg is the Executive Director at SCCWRP, he contributed project management, coordination with stakeholders, and reviewed the final draft.

Acknowledgements

The authors thank field sampling and laboratory personnel from the following organizations: City of San Diego, Orange County Sanitation District, Los Angeles County Sanitation Districts, and the Southern California Coastal Water Research Project. We also want to thank members of the Southern California Bight 2013 Regional Marine Monitoring Program Nutrients and Water Quality Committee who contributed thoughtful comments on study design, data analysis and interpretation, and thoughtful comments on early drafts of this manuscript.

Funding Information

Funding for this project was provided from Orange County Sanitation District, Los Angeles County Sanitation Districts, and the Southern California Coastal Water Research Project.

Competing Interests/ Conflicts of Interest

Dr. Martha Sutula is an editor in the Ecology and Earth Systems Domain and the lead author's husband, Dr. Steven Allison, is Editor-in chief for that same Domain.

Data Accessibility

This study was done in collaboration with the Southern California Bight Regional Marine Monitoring Program, a collaborative monitoring program whose goal is to collect regional-scale data on the health of coastal habitats that can be used to make better management decisions. Pursuant to this goal, all data will be made publicly available on SCCWRP's website: www.sccwrp.org

1 **Table 1. Site information.**

Station ID	Site Description	Region Category	Periods Sampled	Latitude/ Longitude	Depth (m)
2903	LACSD Ocean Outfall	Nearfield	All	33.698/ -118.336	60
3053	LACSD Off-Outfall (northern current)	Nearfield	Summer 2014	33.730/ -118.402	60
3003	LACSD Off-Outfall (northern current)	Nearfield	Spring 2015	33.757/ -118.441	60
2803	LACSD Off-Outfall (southern current)	Nearfield	Summer 2015 Spring 2016	33.668/ -118.297	60
2602	Long Beach Harbor Shelf (LA County)	Nearfield	All	33.694/ -118.191	23
2205	OCSO Ocean Outfall	Nearfield	All	33.576/ -118.005	57
2306	OCSO Off-Outfall (northern current)	Nearfield	Summer 2014	33.581/ -118.052	114
2103	OCSO Off-Outfall (southern current)	Nearfield	Spring 2015 Summer 2015 Spring 2016	33.585/ -117.945	110
1903	Orange County Southern Transect Line	Nearfield	All	33.546/ -117.836	100
CP1	Camp Pendleton- on shelf	Farfield Coastal	All	33.215/ -117.481	65
CP2	Camp Pendleton- continental slope	Farfield Coastal	All	33.184/ -117.523	430
SPOTS	San Pedro Ocean Time Series (LA County Offshore)	Farfield Offshore	All	33.607/ -118.409	730
90.30	CALCOFI station 90 30 (Orange County Offshore)	Farfield Offshore	All	33.419/ -117.912	580

2
3
4

1 **Table 2. Nutrient properties of OCSD and LACSD wastewater effluent. Isotope samples for**
2 **Aug 2015 and Mar 2016 were not analyzed.**

Agency	LACSD				OCSD			
Season	Aug-14	Mar-15	Aug-15	Mar-16	Aug-14	Mar-15	Aug-15	Mar-16
Discharge Rate (MGD)	268	263	257	256	125	119	92	93
PO₄ (μM)	5.5	5.3	3.8	3.5	23.4	34.6	26.5	24.2
NO₂ (μM)	3.9	6.1	15.1	6.2	196	238	152	170
NO₃ (μM)	5.1	4.2	10.5	6.5	883	852	784	850
NH₄ (μM)	2690	3460	2670	1260	1890	1460	1800	2990
DIN	2699	3470	2695	1273	2969	2550	2736	4010
DIN Loading (g/day)	3.8 x10 ⁷	4.8 x10 ⁷	3.7 x10 ⁷	1.7 x10 ⁷	1.9 x10 ⁷	1.6 x10 ⁷	1.3 x10 ⁷	2.0 x10 ⁷
N:P	490	652	1540	852	127	74	103	94
DOC (μM)	1107	1174	1379	1918	1186	1129	1497	2241
DIC (μM)	4900		4361	2750	5076	6398	4404	2909
δ¹⁵N_{NO3} (‰)	-9.6	-2.3			9.1	7.5		
δ¹⁸O_{NO3} (‰)	-15.2	-15.6			-5.8	-3.5		
δ¹⁵N_{NH4} (‰)	7.5	5.1	9.6	12.4	9.1	8.9	8.6	9.1
ε_{nit}	-17.1	-7.4			0	-1.9		

3
4
5

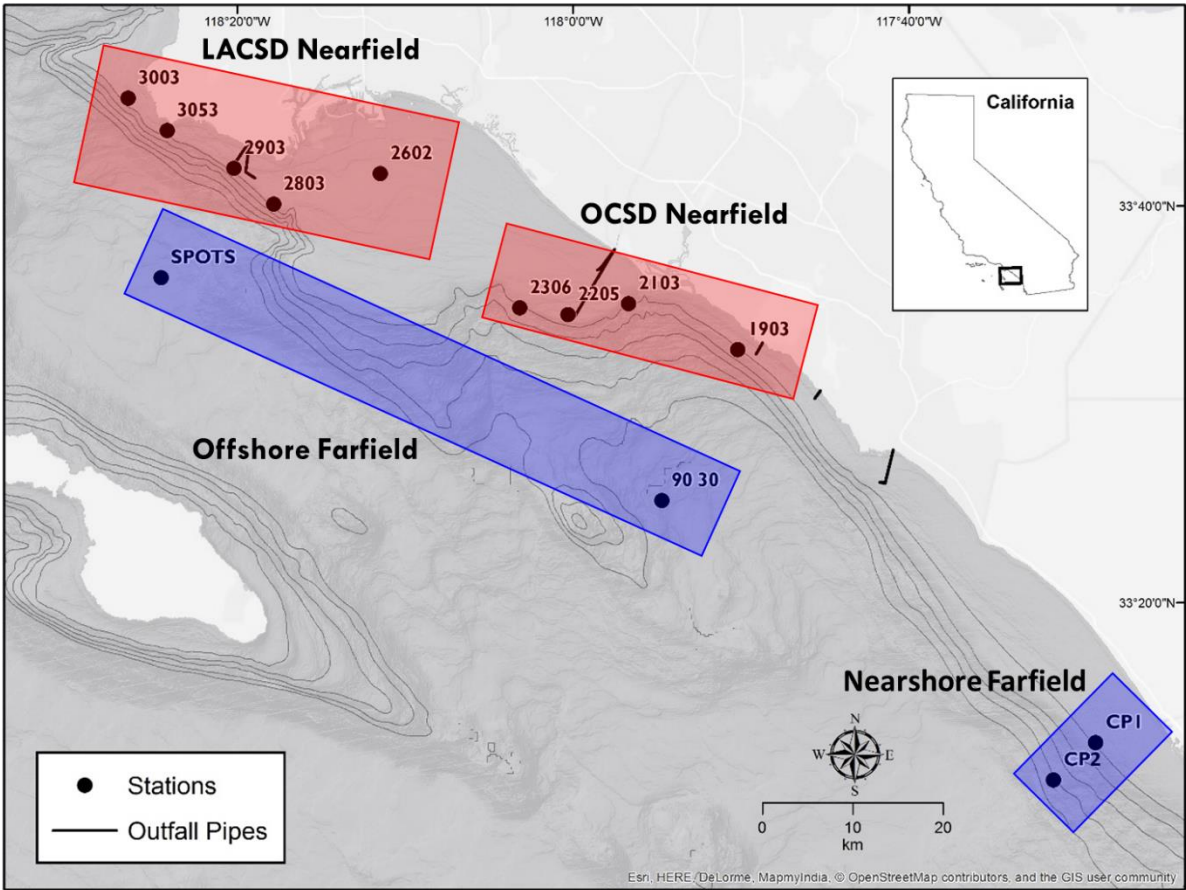
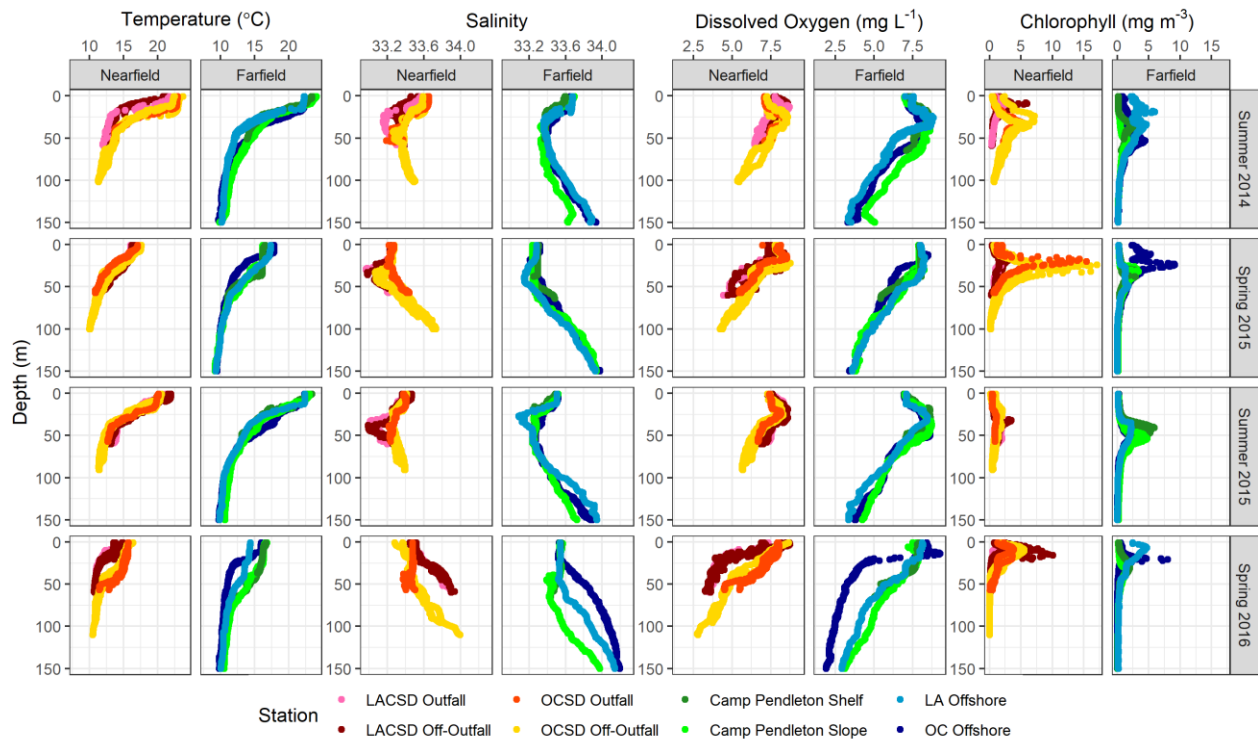


Figure 1. Station Locations. The nearfield sub-regions are shown in red and include LACSD and OCSD grid stations. The farfield (reference) sub-regions spatially distant from the outfalls are shown in blue and include 2 offshore stations (SPOTS and CalCOFI 90.30) and 2 nearshore stations located by Camp Pendleton, in northern San Diego County (CP1 and CP2). CTD casts were collected at additional stations within the regulatory monitoring grids around both LACSD's and OCSD's ocean outfalls to determine the location of the plume at the time of sampling to select the second plume station.

1



2

3 **Figure 2. Spatial and temporal patterns in temperature, salinity, dissolved oxygen, and**
 4 **chlorophyll during each sampling event. Figure is faceted by nearfield stations and farfield**
 5 **stations for each parameter and by season. Each subregion was sampled in a different week**
 6 **in a single month, introducing some temporal variability into the dataset within a season.**

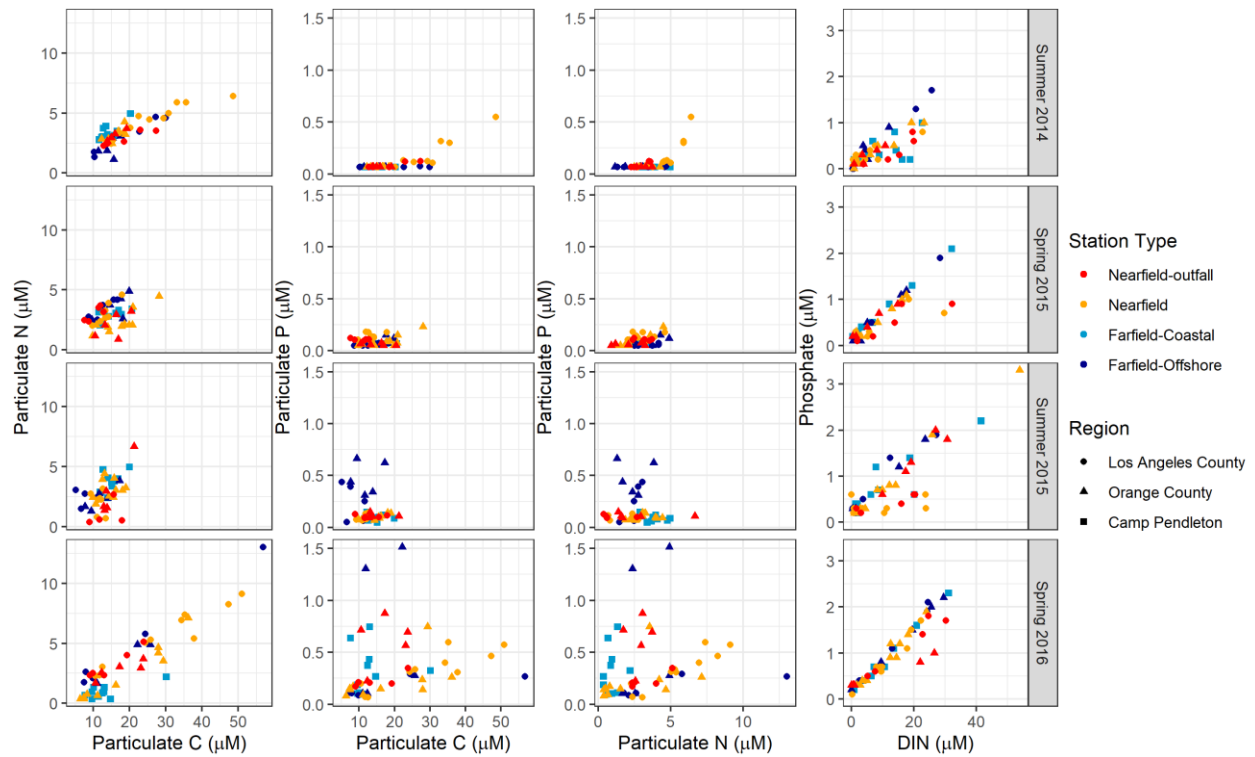
7

8



Figure 3. Depth profiles of dissolved inorganic phosphate, ammonia, nitrite, and nitrate.

1



2

3 **Figure 4. Property-property plots for dissolved and particulate nutrients. Particulate carbon**
 4 **as a function of particulate nitrogen and particulate phosphorus, particulate nitrogen as**
 5 **a function of particulate phosphorus, and dissolved inorganic nitrogen (DIN) as a function of**
 6 **dissolved phosphate.**

7

8

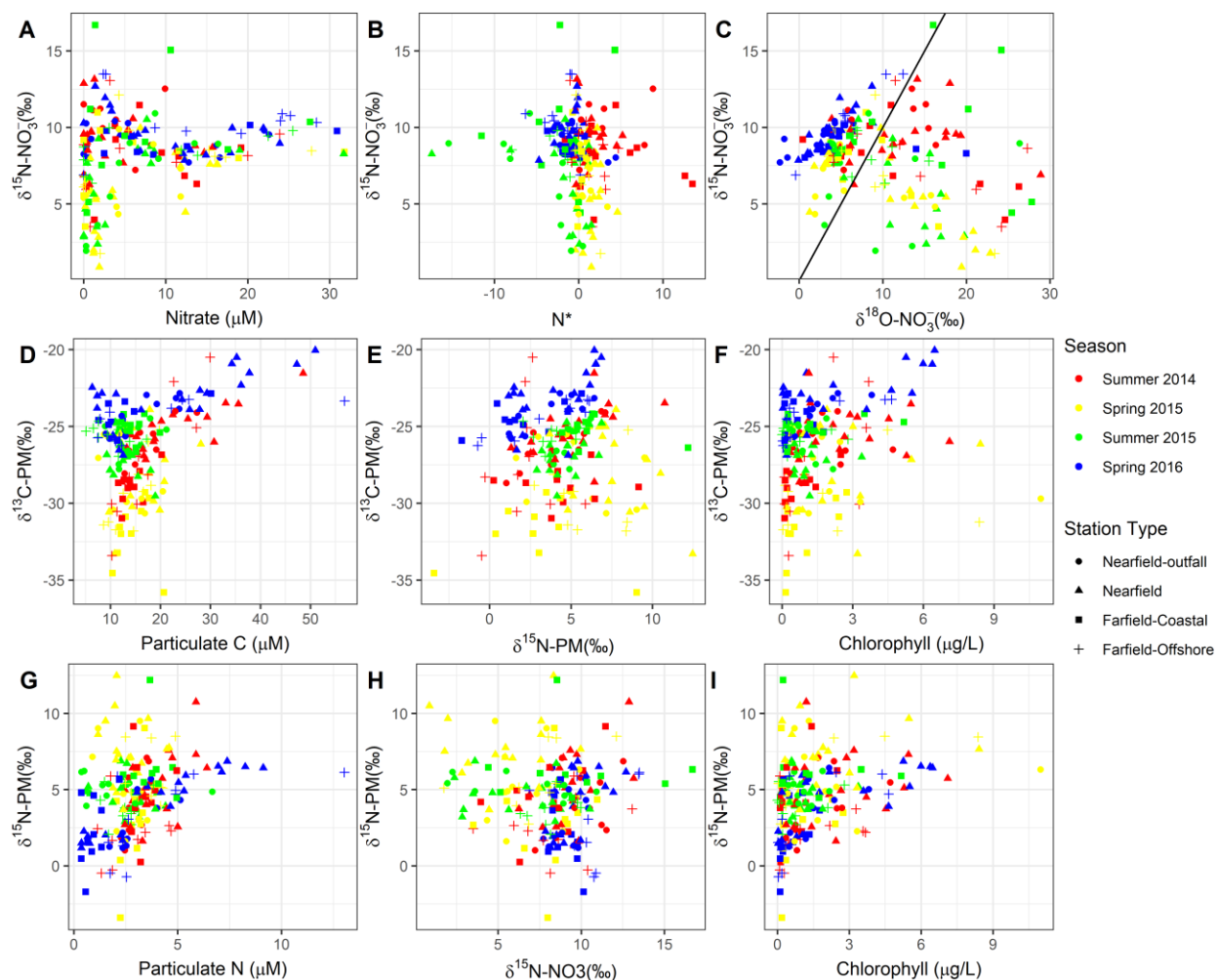


Figure 5. Property-property plots of $\delta^{15}\text{N}_{\text{NO}_3}$ and nitrate concentration (A), $\delta^{15}\text{N}_{\text{NO}_3}$ and N^* (B), and $\delta^{15}\text{N}_{\text{NO}_3}$ and $\delta^{18}\text{O}_{\text{NO}_3}$, where the black line represents 1:1 (C), $\delta^{13}\text{C}_{\text{PM}}$ and particulate carbon concentration (D), $\delta^{13}\text{C}_{\text{PM}}$ and $\delta^{15}\text{N}_{\text{PM}}$ (E), $\delta^{13}\text{C}_{\text{PM}}$ and chlorophyll a (F), $\delta^{15}\text{N}_{\text{PM}}$ and particulate nitrogen concentration (G), $\delta^{15}\text{N}_{\text{PM}}$ and $\delta^{15}\text{N}_{\text{NO}_3}$ (H), $\delta^{15}\text{N}_{\text{PM}}$ and chlorophyll a (I). Colors represent the seasons; shapes represent the station types.

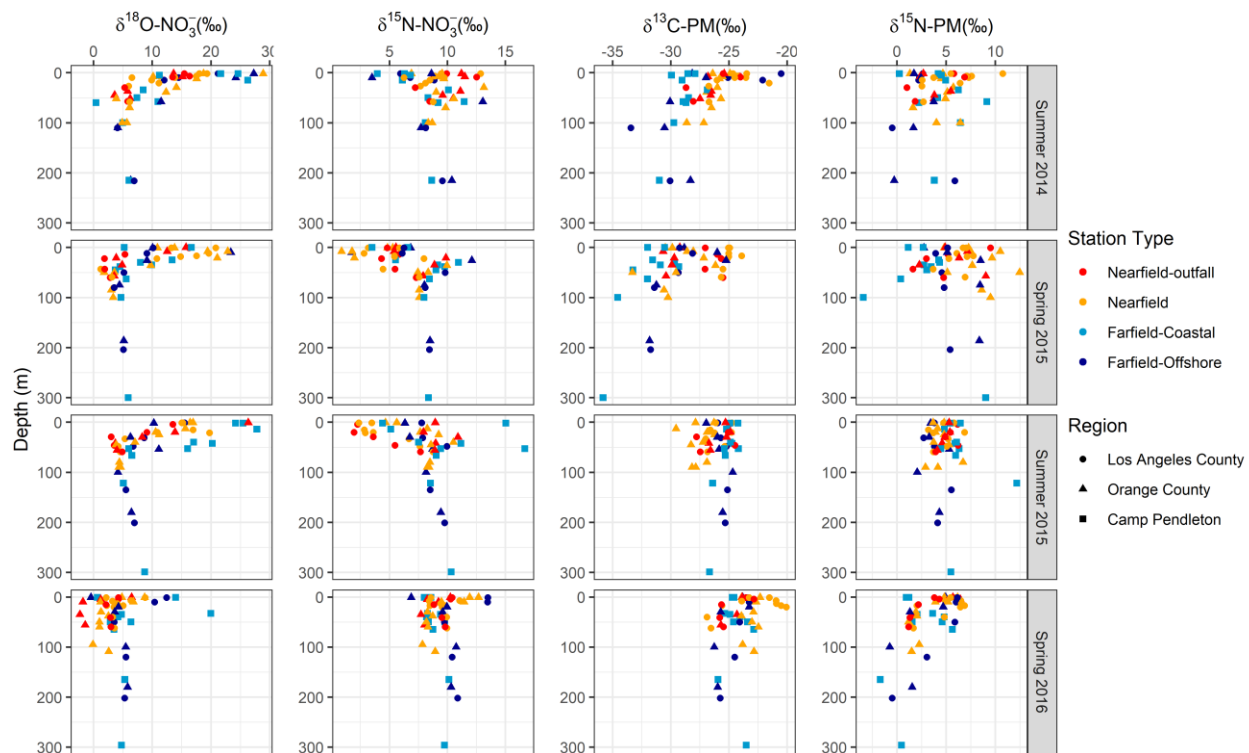


Figure 6. Depth profiles of dissolved $\delta^{15}\text{N}_{\text{NO}_3}$ and $\delta^{18}\text{O}_{\text{NO}_3}$, and particulate $\delta^{13}\text{C}_{\text{PM}}$ and $\delta^{15}\text{N}_{\text{PM}}$.

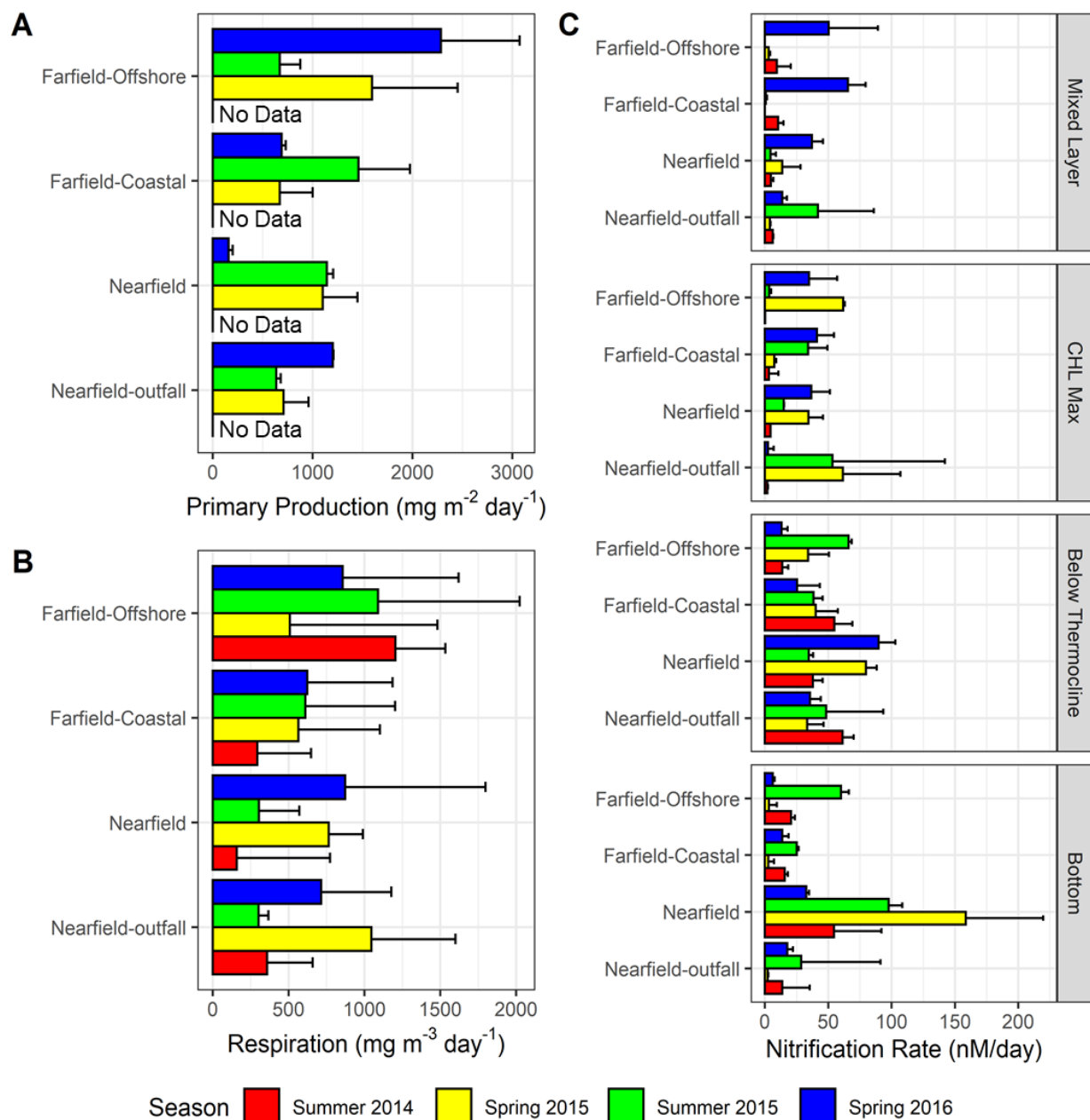


Figure 7. Depth integrated primary production rates (A), average subsurface respiration rates (B), and nitrification rates faceted by depth layer (C) by station type. There was no data collected of primary production in Summer 2014. Error bars for indicate the standard deviation.

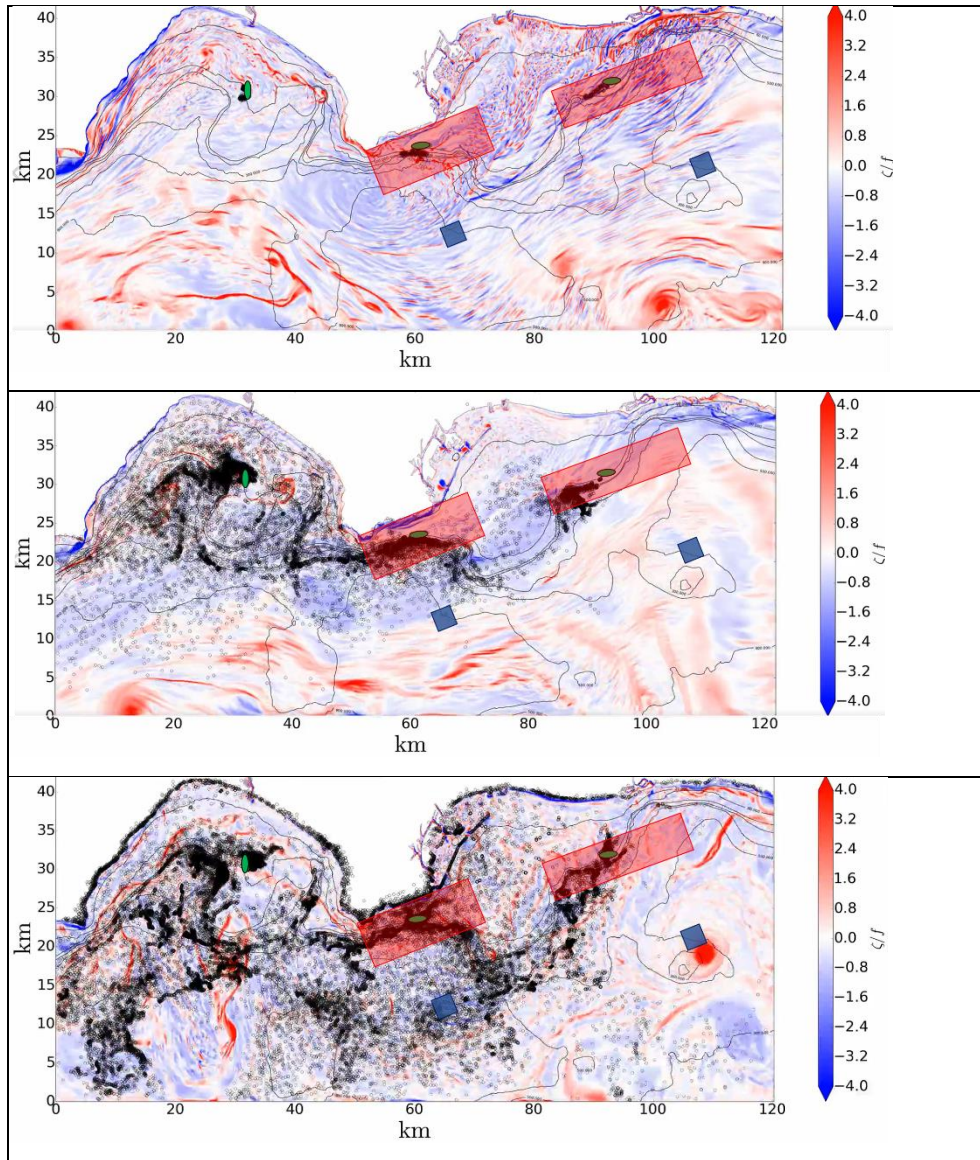


Figure 8. Downscaled Regional Ocean Model (350 m scale) run in particle tracking mode demonstrating the fate of wastewater effluent released from ocean outfalls. Color bar represents the Coriolis-normalized vorticity (a measure of ocean stirring). Black circles represent particles released from outfalls (green ovals). Red boxes are nearfield areas and blue boxes represent farfield, offshore areas. Panel A shows particle distribution 9 hours from the start of the simulation on January 1 at 01:00). Two weeks into the simulation, particles are nearly completely mixed in the nearshore areas (Panel B). Panel C shows the end of the simulation, two months, particles released from the outfalls have been mixed to the offshore regions (Dauhajre et al. 2019).

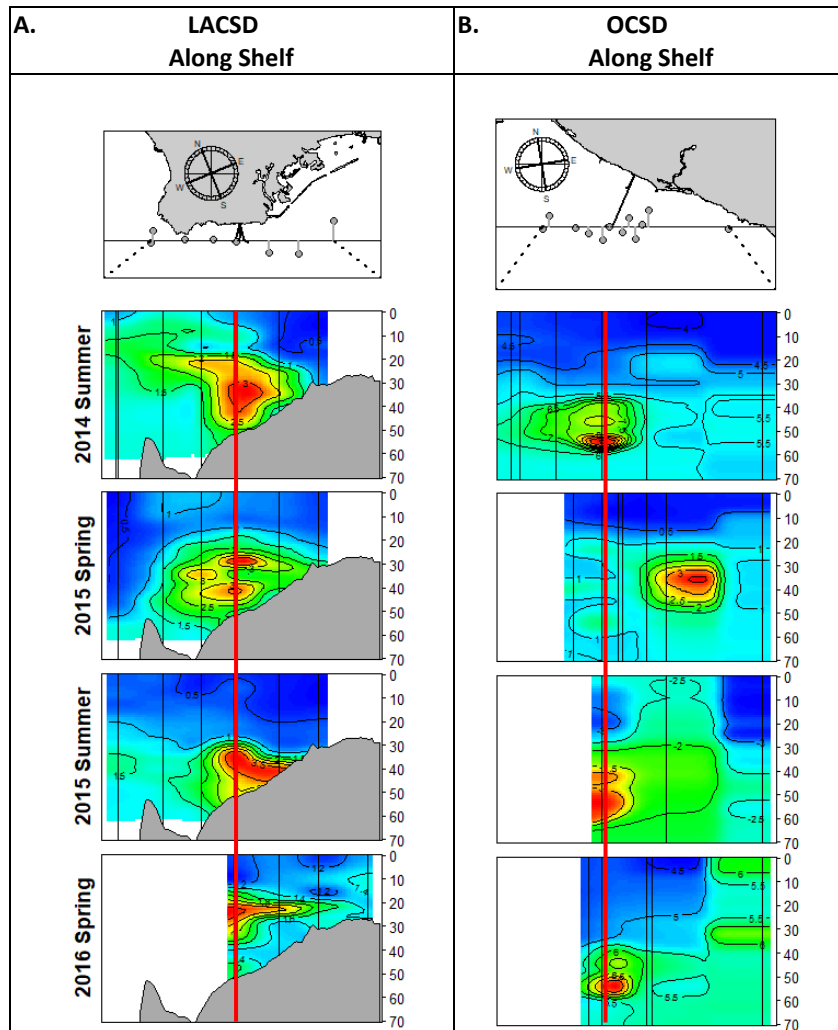


Figure SI.1. Spatial extent of the effluent plumes during each of the sampling events as measured by CDOM (mg m^{-3}). Note colored scale on each graphic is different, scaling was free on each figure to demonstrate the extent of the plume. Scales are plotted from the minimum reported value to the maximum for each site to identify the plume locations over each outfall. Each CTD cast location is represented by a black vertical line, multiple casts were taken to determine the direction of the plume during sampling events and not all stations correspond to sampling locations on Figure 1. The station sampled over each outfall is highlighted in red.

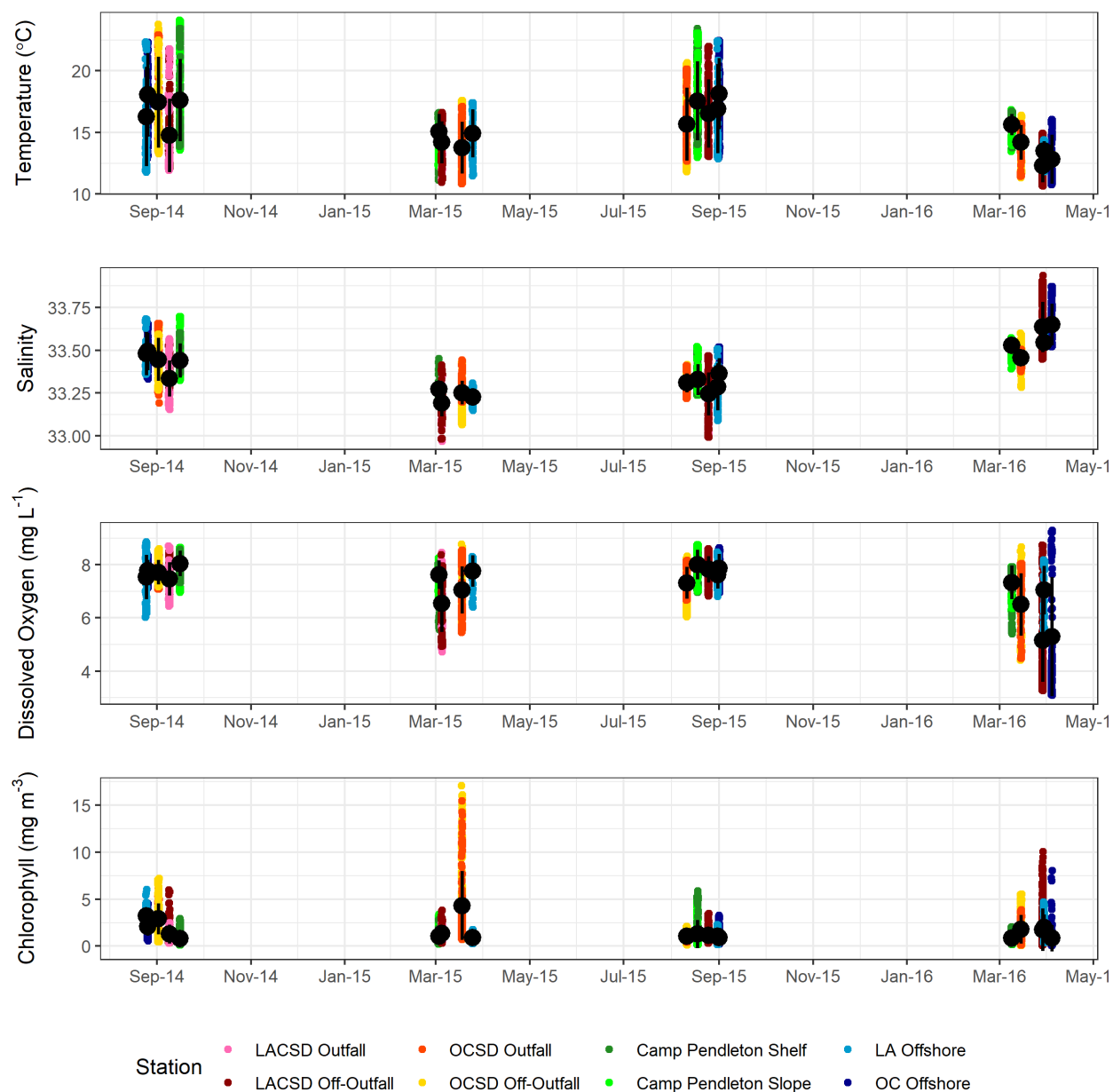


Figure SI.2. Timing of sampling and ranges of data for upper 60 m at each site. Black dot represents the mean and bar the standard deviation of all values in upper 60 m.

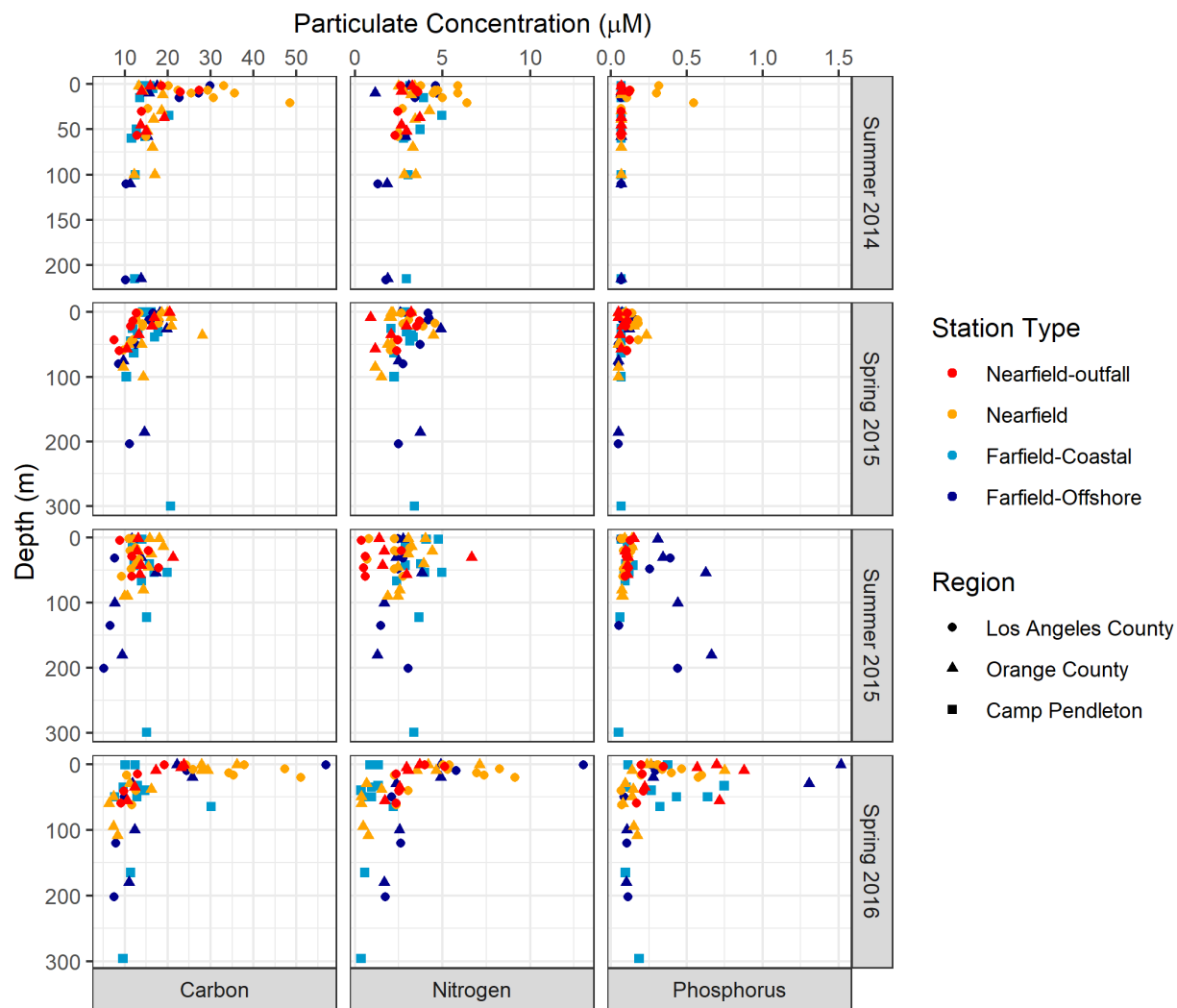


Figure SI.3. Depth profiles of particulate carbon, nitrogen and phosphorus.

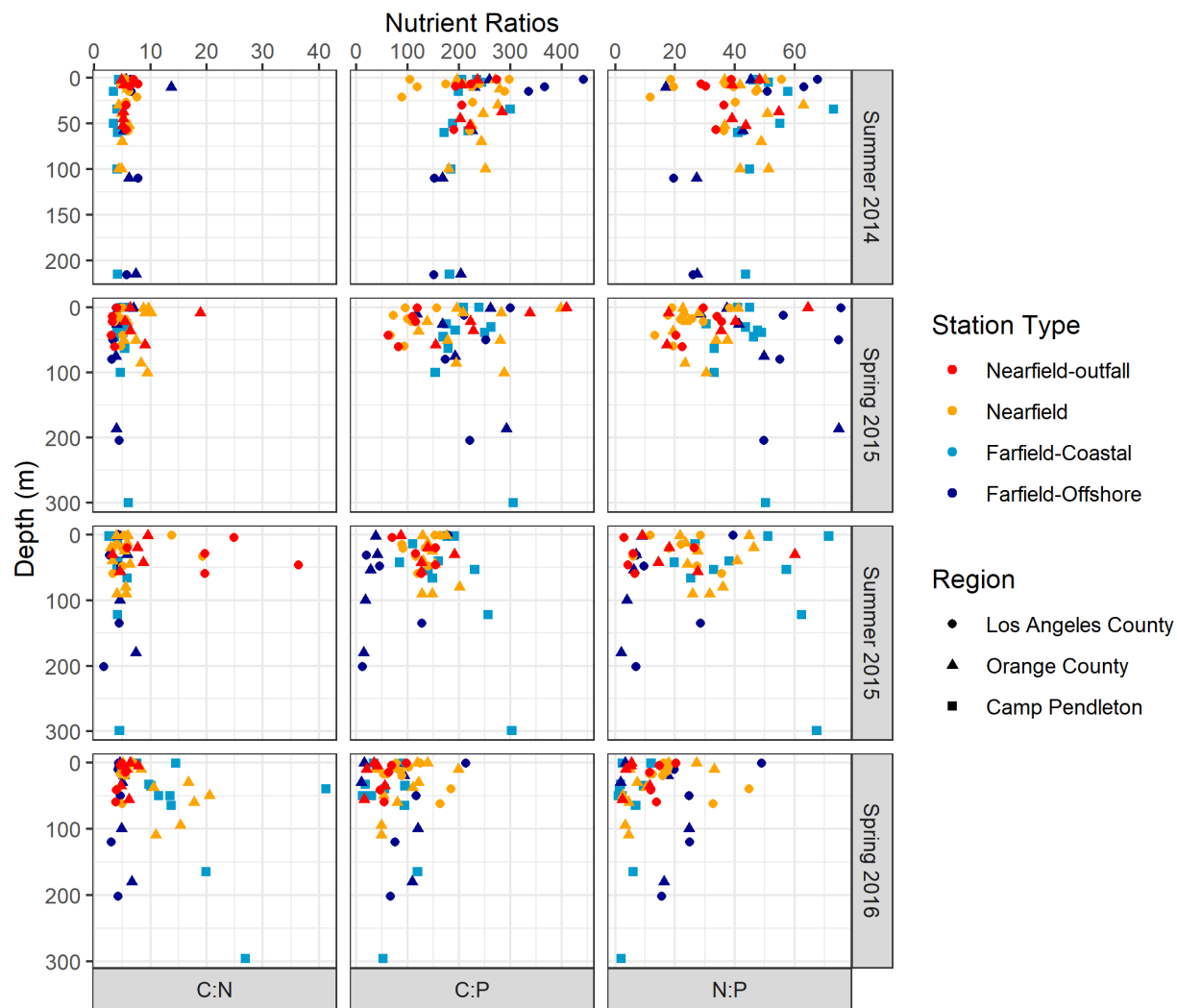


Figure SI.4. Depth profiles of particulate C:N, C:P, and N:P.

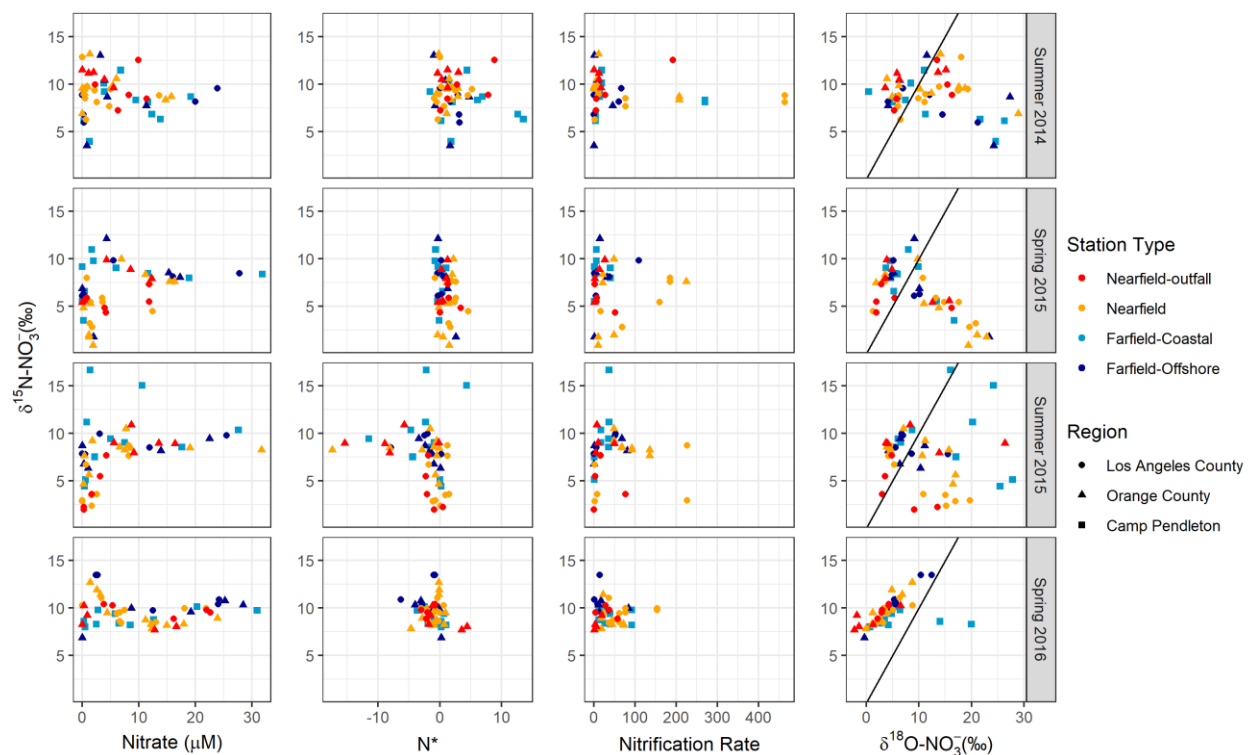


Figure SI.5. The $\delta^{15}\text{N}_{\text{NO}_3}$ as a function of nitrate concentration, N^* , nitrification rate, and $\delta^{18}\text{O}_{\text{NO}_3}$. The black line in the final column represents a 1:1 relationship between the relative enrichment of the two isotopes.

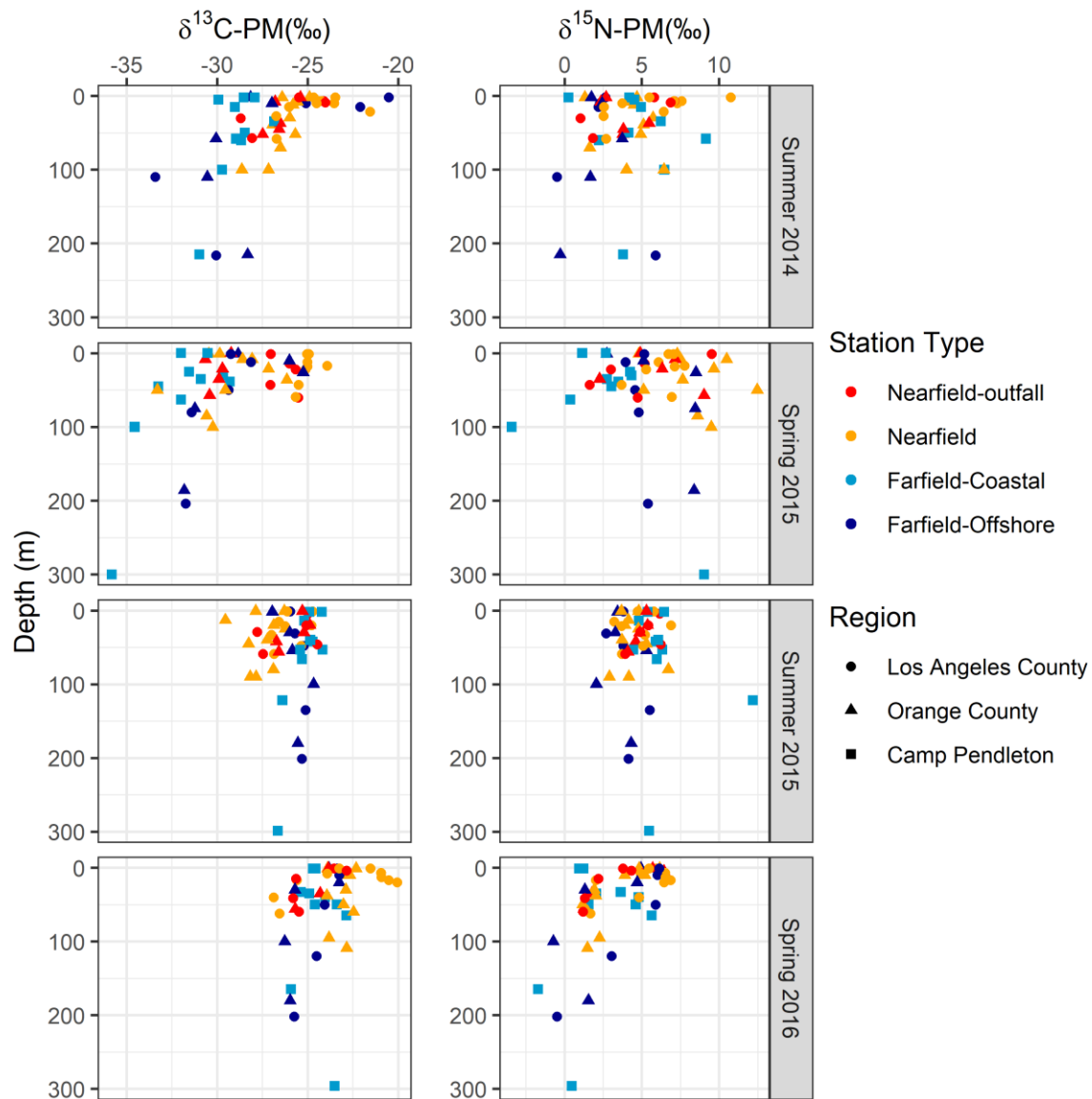


Figure SI.6. Depth profiles of the stable isotopic composition of particulate carbon ($\delta^{13}\text{C}_{\text{PM}}$) and nitrogen ($\delta^{15}\text{N}_{\text{PM}}$).

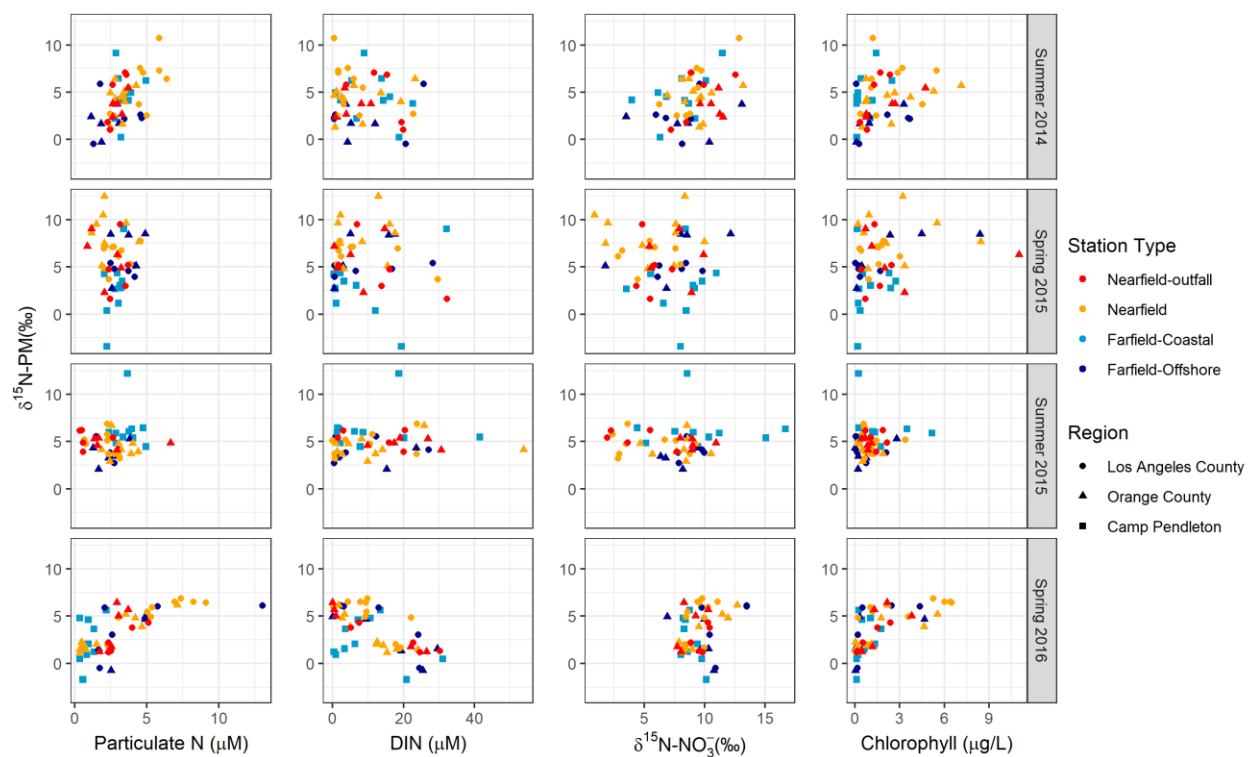


Figure SI.7. The $\delta^{15}\text{N}_{\text{PM}}$ as a function of particulate nitrogen concentration, dissolved inorganic nitrogen (DIN), $\delta^{15}\text{N}_{\text{NO}_3^-}$, and chlorophyll a concentration.

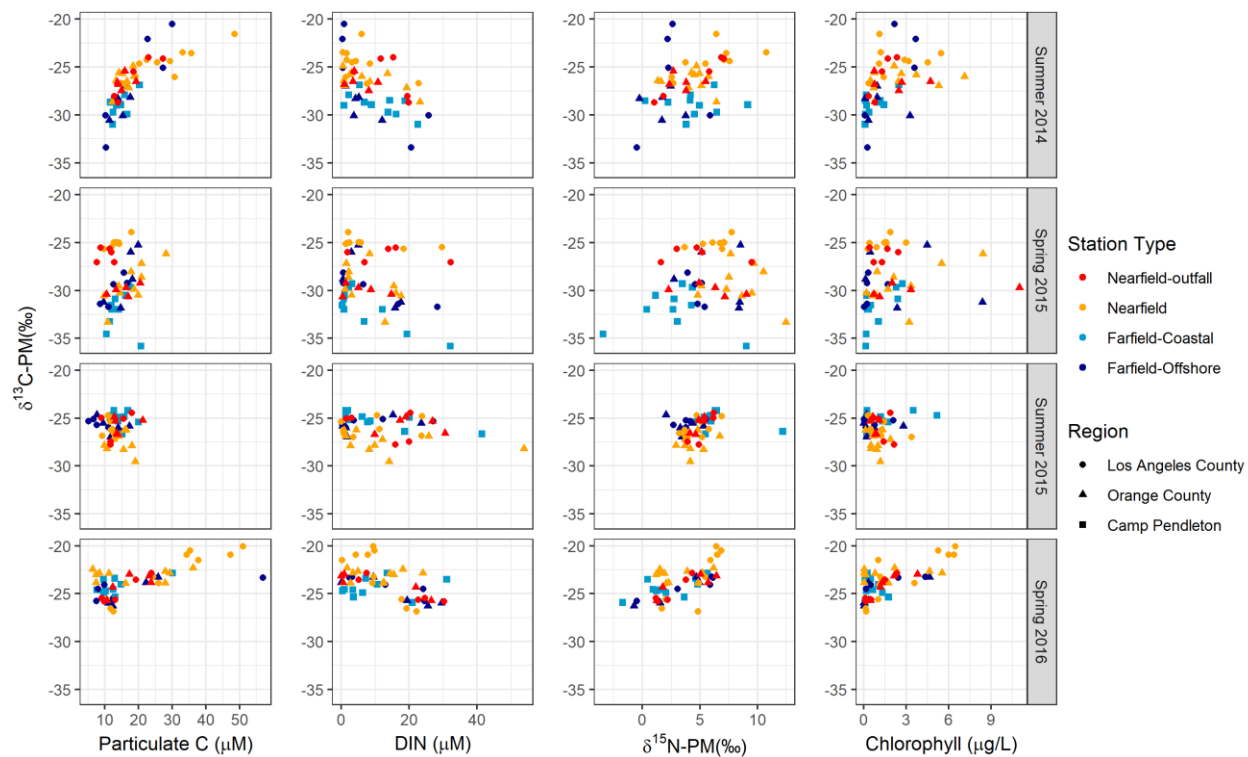


Figure SI.8. $\delta^{13}\text{C}_{\text{PM}}$ as a function of particulate carbon, DIN, $\delta^{15}\text{N}_{\text{PM}}$, and chlorophyll a concentration.

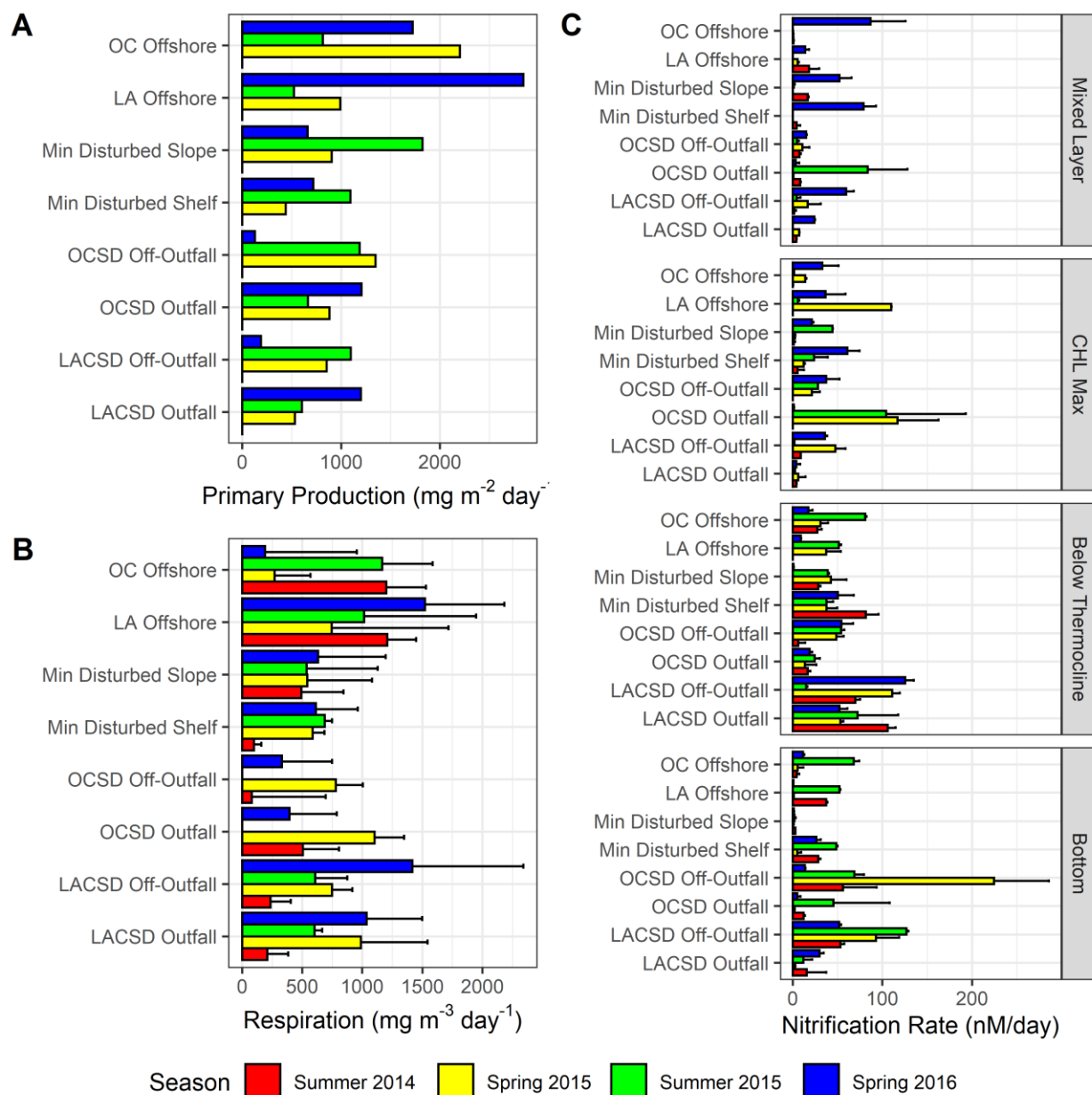


Figure SI.9. Depth integrated primary production rates (A), average subsurface respiration rates (B), and nitrification rates faceted by depth layer (C) by station. There was no data collected of primary production in Summer 2014. Error bars for indicate the standard deviation.

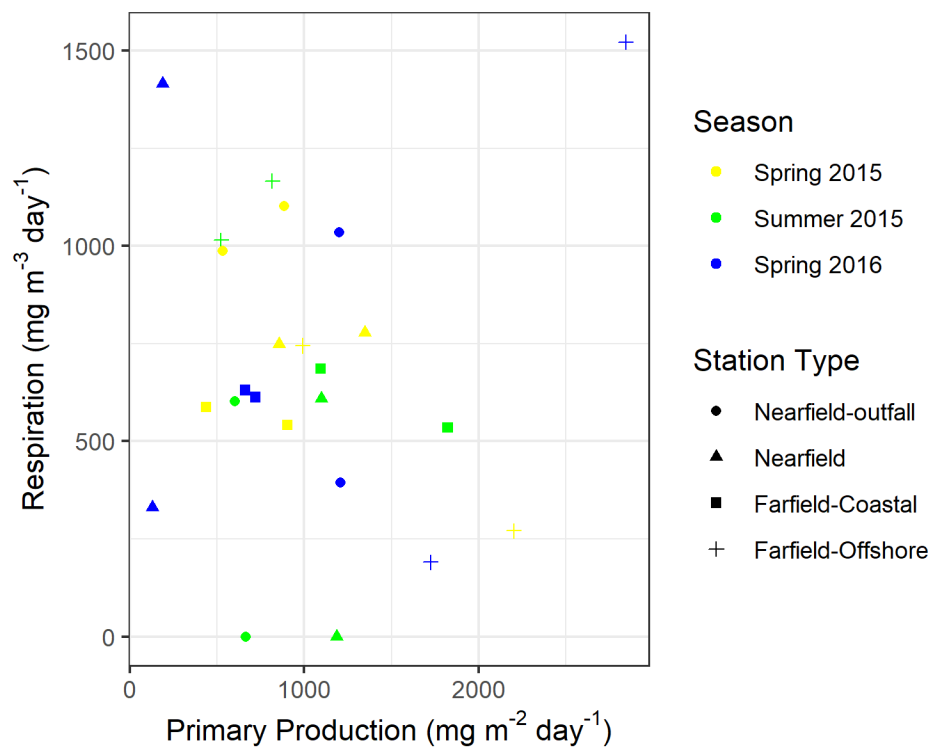
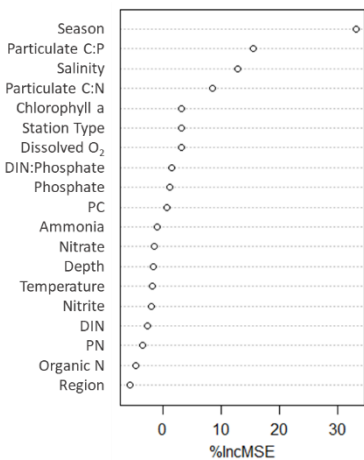
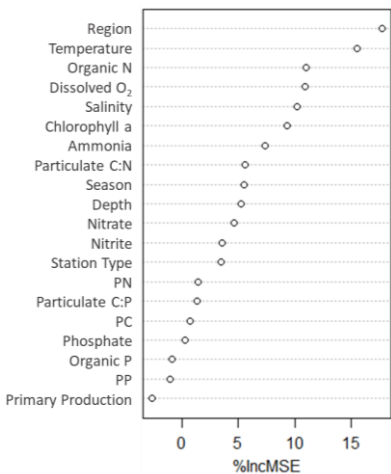


Figure SI.10 Relationship between depth integrated primary production and average subsurface respiration for the three-time periods when both parameters were measured.

A. Primary Production



B. Respiration



C. Nitrification

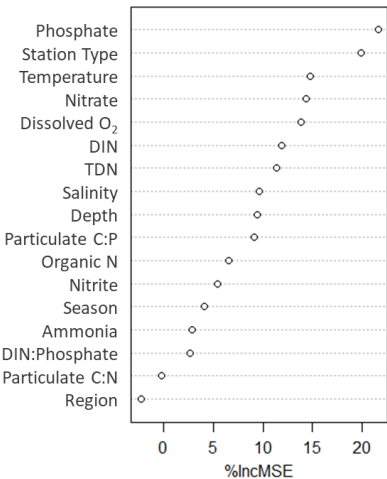


Figure SI.11. Variable importance from random forest regression models predicting primary production (A), respiration (B), and Nitrification (C). Predictor variables were plotted with their increase in percent mean squared error (%IncMSE) when the variable is randomly permuted in the model, higher values indicate variables were more important to the regression. The overall percent variance explained using the random forest models was 30% for primary production, 18% for respiration, and 20% for nitrification.